ALEX(01)-TR-78-07

LEVEL II

12

FEASIBILITY STUDY OF MIXED-SIGNAL SEPARATION TECHNIQUES

TECHNICAL REPORT NO. 10
VELA NETWORK EVALUATION AND AUTOMATIC PROCESSING RESEARCH

Prepared by
Wen-Wu Shen

TEXAS INSTRUMENTS INCORPORATED
Equipment Group
Post Office Box 6015
Dallas, Texas 75222

Prepared for

AIR FORCE TECHNICAL APPLICATIONS CENTER
Alexandria, Virginia 22314

Sponsored by

ADVANCED RESEARCH PROJECTS AGENCY
Nuclear Monitoring Research Office
ARPA Program Code No. 7T10
ARPA Order No. 2551

12 July 1978

Acknowledgment: This research was supported by the Advanced Research Projects Agency, Nuclear Monitoring Research Office, under Project VELA-UNIFORM, and accomplished under the technical direction of the Air Force Technical Applications Center under Contract Number F08606-77-C-0006.

APPROVED FOR PUBLIC RELEASE, DISTRIBUTION UNLIMITED

ALEX(01)-TR-78-07

FEASIBILITY STUDY OF MIXED-SIGNAL SEPARATION TECHNIQUES

TECHNICAL REPORT NO. 19
VELA NETWORK EVALUATION AND AUTOMATIC PROCESSING RESEARCH

Prepared by
Wen-Wu Shen

TEXAS INSTRUMENTS INCORPORATED
Equipment Group
Post Office Box 6015
Dallas, Texas 75222

Prepared for

AIR FORCE TECHNICAL APPLICATIONS CENTER
Alexandria, Virginia 22314

Sponsored by

ADVANCED RESEARCH PROJECTS AGENCY
Nuclear Monitoring Research Office
ARPA Program Code No. 7F10
ARPA Order No. 2551

12 July 1978

Acknowledgment: This research was supported by the Advanced Research Projects Agency, Nuclear Monitoring Research Office, under Project VELA-UNIFORM, and accomplished under the technical direction of the Air Force Technical Applications Center under Contract Number F08606-77-C-0004.

UNCLASSIFIED

SECURITY CLASSIFICATION OF THIS PAGE (When Data Entered)

REPORT DOCUMENTATION PAGE		READ INSTRUCTIONS BEFORE COMPLETING FORM
1. REPORT NUMBER	2. GOVT ACCESSION NO.	3. RECIPIENT'S CATALOG NUMBER
4. TITLE (and Subtitle) (6) FEASIBILITY STUDY OF MIXED-SIGNAL SEPARATION TECHNIQUES.		5. TYPE OF REPORT & PERIOD COVERED (9) Technical rept. no. 19
		6. PERFORMING ORG. REPORT NUMBER (14) ALEX(01)-TR-78-07
7. AUTHOR(s) (10) Wen-Wu Shen		8. CONTRACT OR GRANT NUMBER(s) F08606-77-C-0004
9. PERFORMING ORGANIZATION NAME AND ADDRESS Texas Instruments Incorporated Equipment Group Dallas, Texas 75222		10. PROGRAM ELEMENT, PROJECT, TASK AREA & WORK UNIT NUMBERS VELA T/8705/B/PMP
11. CONTROLLING OFFICE NAME AND ADDRESS Advanced Research Projects Agency Nuclear Monitoring Research Office Arlington, Virginia 22209		12. REPORT DATE (11) 12 July 1978 13. NUMBER OF PAGES 59 (12) 61 p.
14. MONITORING AGENCY NAME & ADDRESS (if different from Controlling Office) Air Force Technical Applications Center VELA Seismological Center Alexandria, Virginia 22314		15. SECURITY CLASS. (of this report) UNCLASSIFIED 15a. DECLASSIFICATION/DOWNGRADING SCHEDULE

16. DISTRIBUTION STATEMENT (of this Report) (15) F08606-77-C-0004, ARPA Order-2551

APPROVED FOR PUBLIC RELEASE, DISTRIBUTION UNLIMITED

17. DISTRIBUTION STATEMENT (of the abstract entered in Block 20, if different from Report)

18. SUPPLEMENTARY NOTES

ARPA Order No. 2551

19. KEY WORDS (Continue on reverse side if necessary and identify by block number)

Mixed-Signal Separation
Real Amplitude Shading
KSRS Short-Period Array
Adaptive Beamformer
Complex Amplitude Shading
Response Pattern

20. ABSTRACT (Continue on reverse side if necessary and identify by block number)

A feasibility study to enhance a weaker signal hidden in the stronger wavetrains of different seismic sources was conducted. Two array beamforming methods were developed for and applied to the mixed-signal problem: one is the adaptive beamformer (ABF) and the other is array shading technique. The ABF operates in the time domain, requires no a priori information, and can be used for a front-end detector. The array shading technique is designed in the frequency domain, needs interfering azimuth for null

DD FORM 1 JAN 73 1473 EDITION OF 1 NOV 65 IS OBSOLETE

UNCLASSIFIED

SECURITY CLASSIFICATION OF THIS PAGE (When Data Entered)

JUB

405 076

20. continued

steering, and is intended for a post-detection processor. Results from experimental tests with recorded data from the Korean Seismic Research Station short-period array are also included.

ABSTRACT

A feasibility study to enhance a weaker signal hidden in the stronger wavetrains of different seismic sources was conducted. Two array beamforming methods were developed for and applied to the mixed-signal problem: one is the adaptive beamformer (ABF) and the other is array shading technique. The ABF operates in the time domain, requires no a priori information, and can be used for a front-end detector. The array shading technique is designed in the frequency domain, needs interfering azimuth for null steering, and is intended for a post-detection processor. Results from experimental tests with recorded data from the Korean Seismic Research Station short-period array are also included.

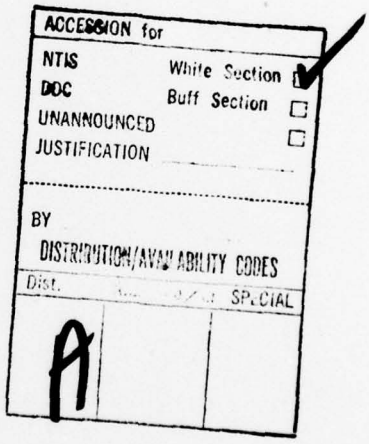

ACKNOWLEDGMENTS

I gratefully thank Mrs. Cherylann B. Saunders for typing the manuscript and preparing the figures.

This research was supported by the Advanced Research Projects Agency, Nuclear Monitoring Research Office under Project VELA-UNIFORM, and was accomplished under the technical direction of the Air Force Technical Applications Center under Contract Number F08606-77-C-0004.

TABLE OF CONTENTS

LIST OF FIGURES

LIST OF FIGURES
(continued)

LIST OF TABLES

SECTION I
INTRODUCTION

In a front-end detection system, when a strong source (earthquakes as specifically discussed here) generates a great amount of energy which lasts a substantial length of time, a detector can be jammed and loses its detection capability or yields excessive false alarms. This problem is more pronounced in a siesmic detection system as earthquakes occur within a distance of 2000 km from the sensors. Our attempts to solve the problem are being made by employing a number of techniques applicable as a front-end detector or as a post-detection processor, respectively.

By employing array beamforming techniques which we developed, we will evaluate the feasibility of using arrays to separate mixed signals which are weak signals occurring after strong signals. They are difficult to detect due to the coda or scattered energy of the preceding stronger signal interfering or overshadowing the later arriving weak signal. The problem here is how to reject the high-amplitude interfering wavetrains of the stronger earthquake and how to extract the weaker hidden signal from the interfering environment.

Two array beamforming techniques were studied for this purpose: one is in the time domain and can be used as a front-end detector and the other in the frequency domain and intended for a post-detection processor. First, we applied to the problem the L_1 norm adaptive beamformer (ABF) which is of time-varying adaptation rate in terms of L_2 norm formulation. The ABF is a time-domain processor and can operate in a real-time and front-end detection system. Secondly, using the formulation of the variational principle we

tried to null-steer the array by the method of weighting the array sensors so that it could reject the stronger interfering wavetrains and extract the hidden weak signal through an array beamforming process. This formulation was in the frequency domain and the technique can be used for a post-detection processor.

The ABF algorithm described by Shen (1977) was modified in this report. Mathematical algorithms for the array-shading technique were formulated, software programs were developed for the computations, and experimental tests on recorded data from the Korean Seismic Research Station (KSRS) short-period array were conducted. Section II presents a brief description of the adaptive beamforming algorithm. Section III describes the physical formulation of array weighting algorithms and their computational results. Experimental procedures and results from the recorded-data tests are presented in Section IV, followed by conclusions and suggestions for further study in Section V. Finally, references are listed in Section VI.

SECTION II

THE ADAPTIVE BEAMFORMER — FRONT-END DETECTOR

A time-domain linear adaptive beamformer (ABF) was developed for use in an operational front-end detection system. The objective is to increase the detection capability of a siesmic array and to extract the low-magnitude signals of unknown waveforms from noise. The algorithm minimizes the squared filter output subject to the constraints which pass energy from steered location. Mathematically, let y(t) be the adaptive filter output at time t for an array of N sensors (channels) with a 2J+1 points, or tappings of filter length per channel. Then, we write

$$y(t) = \sum_{j=1}^{N} \sum_{n=-J}^{J} a_j(n)\, X_j(t-n\Delta t) \qquad (II\text{-}1)$$

where X_j is time-aligned data input for the j^{th} channel, Δt is the sampling interval, and $a_j(n)$ is the adaptive filter coefficient for the j^{th} channel and n^{th} tapping (filter point) of the sensor. In the algorithm, $a_j(n)$ is iterated, or updated in the time-domain by the expression

$$a_j^{t+\Delta t}(n) = a_j^{t}(n) + \mu\lambda(t)\, y(t) \left[\overline{X}(t-n\Delta t) - X_j(t-n\Delta t) \right] \qquad (II\text{-}2)$$

where $a_j(n)$ is initialized to satisfy the Levin's constraints (Levin, 1964)

$$\sum_{j=1}^{N} a_j(n) = \delta_{no} \qquad (II\text{-}3)$$

for a center point output described in equation (II-1) and where

$$\bar{X}(t-n\Delta t) = \frac{1}{N}\sum_{j=1}^{N} X_j(t-n\Delta t) \qquad \text{(II-4)}$$

$\bar{X}$ is introduced to preserve the constraints which were initialized at the very beginning of processing. The algorithm was formulated (with $\lambda(t) = 1.0$) by Burg et al. (1967) and has been investigated by various authors (Kobayashi, 1970; Frost, 1972; Owsley, 1973; and Gangi and Byun, 1976). The algorithm achieves a substantial noise reduction gain relative to the beamsteer (time-align and average) processor. However, experimental work on the recorded seismic data indicated a substantial signal loss compared with the beamsteer output. That resulted in the optimum signal-to-noise ratio (SNR) gain around 1 dB relative to the beamsteer processor.

A better time-domain adaptation is needed to achieve a better SNR gain. It was found that a quasi L_1 norm adaptive filter improved the performance both in reducing the noise and in preventing the desired signal from being degraded (Shen, 1977). Currently, the L_1 norm ABF has been modified in an attempt to make the ABF processor implementable for optimum operation in various levels of noise environment. Presently, the time-varying adaptation rate, $\lambda(t)$ is chosen as follows:

$$\lambda(t) = \frac{\bar{y}_{LTS}(t)}{\bar{y}_{STS}(t) \times P(t)} \qquad \text{(II-5)}$$

where

$$\bar{y}_{LTS}(t) = (1-\alpha)\,\bar{y}_{LTS}(t-1) + \alpha|y(t)| \qquad \text{(II-6)}$$

$$\bar{y}_{STS}(t) = (1-\beta)\,\bar{y}_{STS}(t-1) + \beta|y(t)| \qquad \text{(II-7)}$$

and

$$P(t) = \sum_{j=1}^{N} \sum_{n=-J}^{J} X_j^2(t-n\Delta t) \qquad \text{(II-8)}$$

α is a long-term smoothing constant of filter output for noise adaptation so that $\bar{y}_{LTS}(t)$ can characterize the noise level in the environment. β is the short-term smoothing constant of filter output intended to prevent the signal loss when $\bar{y}_{STS}(t)$ increases. The introduction of $\bar{y}_{LTS}(t)$ and $\bar{y}_{STS}(t)$ is intended to fix μ for the detector so that it can operate in different noise environments. It is noted that the performance of the adaptive beamformer is highly dependent on α, β, and μ.

SECTION III

AMPLITUDE SHADING OF ARRAY SENSORS — POST-DETECTION PROCESSOR

A. INTRODUCTORY REMARKS

The Dolph-Chebyshev technique is often applied to compute the coefficients for array sensors. It gives the minimum width of mainlobe for a given response of minor lobes or gives the minimum response of minor lobes for a given width of mainlobe. The purpose of the computation is to obtain an array directional response so that a signal being searched or estimated can be enhanced from the noise environment. The technique was first developed by Dolph (1946) who expanded the pattern function to the appropriate Chebyshev polynomials and obtained an analytical solution of the coefficients (or weightings) for array sensors. However, the analytical approach has the disadvantage that it is limited to simple configurations of sensors such as equally spaced line arrays, rectangular arrays, or circular arrays.

For the mixed-signal separation problem which we addressed in this report, we tried to obtain the directional steering of an array to the desired signal and simultaneously attempted to create a 'null' response for the array in the direction of an unwanted interfering signal. By doing so, the desired signal could pass the array beamforming processor without being distorted, and on the other hand, the interfering energy could be reduced or eliminated by filtered array beamforming. Because it is not designed to void the array response in a specific direction, the Dolph-Chebyshev method can not be applied in this case, even if simple geometry of the array is employed. Furthermore, the Dolph-Chebyshev method, which minimizes the maximum side lobe response of arrays of simple

geometry, cannot be applied to arbitrary sensor configurations which typify seismic arrays. In light of the difficulties the analytical method encountered, one has to rely on a more general numerical approach. A digital computer perfectly serves the purpose of determining the null-steer coefficients required to optimize mixed-signal separation.

In this section, a numerical method will be demonstrated in which we applied the variational principle to minimize the total array power response subject to filter weight constraints. The physical model we used is an isotropic noise and two propagating signals - one for the signal being sought and the other for the stronger interfering signal to be eliminated.

B. PHYSICAL FORMULATION

1. Real Amplitude Weighting Algorithm

a. Amplitude and Power Pattern Received by an Array

The configuration of array sensors considered here is two-dimensional and is on the earth's surface. Let the j^{th} sensor of an array be located at (r_j, ϕ_j) in polar coordinates and a wave of single frequency with wavenumber k ($=2\pi f/v$, where f is frequency and v is apparent phase velocity) be incident on the array from azimuthal angle ϕ. The amplitude pattern received by the array of N sensors is expressed as

$$F(k, \phi, \phi_o) = \sum_{j=1}^{N} e^{i\left[kr_j \cos(\phi - \phi_j) - kr_j \cos(\phi_o - \phi_j)\right]} \qquad \text{(III-1)}$$

where

$i = \sqrt{-1}$, and

ϕ_o = the steering azimuth of the array, or the direction of a desired signal to be searched or estimated.

In the seismic community, the azimuthal angle is usually referenced to the geographical North in clockwise rotation, but equation (III-1) should not be changed because cosine is an even function. Also, equation (III-1) is the beamsteer (evenly weighted) amplitude pattern of the array. The real amplitude shading (weighting) is meant to multiply each array sensor by a real number (or coefficient) to achieve a certain design goal. Hence we re-write equation (III-1) in the form where the j^{th} sensor is to be weighted by a real number a_j such that

$$F(k, \phi, \phi_o) = \sum_{j=1}^{N} a_j e^{i\left[kr_j\cos(\phi-\phi_j) - kr_j\cos(\phi_o-\phi_j)\right]} . \quad \text{(III-2)}$$

Consequently, the array beam power pattern is

$$\begin{aligned} P(k, \phi, \phi_o) &= F(k, \phi, \phi_o)\, F^*(k, \phi, \phi_o) \\ &= \sum_{\ell=1}^{N}\sum_{j=1}^{N} a_j a_\ell e^{i\left[kr_j\cos(\phi-\phi_j) - kr_j\cos(\phi_o-\phi_j)\right.} \\ &\quad \left. - kr_\ell\cos(\phi-\phi_\ell) + kr_\ell\cos(\phi_o-\phi_j)\right] \end{aligned} \quad \text{(III-3a)}$$

or

$$P(k, \phi, \phi_o) = \sum_{j=1}^{N} a_j^2 + 2\sum\sum_{\ell > j} a_j a_\ell C_{\ell j} \quad \text{(III-3b)}$$

where

$$\begin{aligned} C_{\ell j} &= \cos\left[kr_j\cos(\phi-\phi_j) - kr_j\cos(\phi_o-\phi_j)\right. \\ &\quad \left. - kr_\ell\cos(\phi-\phi_\ell) + kr_\ell\cos(\phi_o-\phi_\ell)\right] . \end{aligned} \quad \text{(III-4)}$$

Normally, the configuration of a seismic array is, in some sense, arbitrary and their sensor locations are expressed in the Cartesian coordinates in which we have

$$x_j = r_j \sin \phi_j$$

and

$$y_j = r_j \cos \phi_j \quad . \tag{III-5}$$

Again, we write $C_{\ell j}$ in equation (III-4) in Cartesian coordinates here

$$C_{\ell j} = \cos\left[k(x_j - x_\ell)(\sin\phi - \sin\phi_o) + k(y_j - y_\ell)(\cos\phi - \cos\phi_o)\right]. \tag{III-6}$$

b. Noise and Signal Model

Power pattern received by the array in equation (III-3) is for a single incident 'ray' of signal or noise. For the problem we addressed in this report, we were essentially concerned with two signals - one is the desired signal to be enhanced and the other is the interfering signal to be reduced or eliminated. In addition to the mixed signals, we added an isotropic noise to the environment for practical realization. Therefore, we have one noise and two signals as the working physical model.

The energy for the isotropic noise should be the integration of equation (III-3b) over the whole two-dimensional space. Let $P_N(k)$ be the power for the noise component. Then we have

$$P_N(k, \phi_o) = \int_0^{2\pi} P(k, \phi, \phi_o)\, d\phi \quad . \tag{III-7a}$$

Equation (III-7a) can be analytically accomplished for certain configurations of array geometry and was elegantly done for a line array and a circular array by Wang (1975, 1977). However, for a seismic array as expressed in equation (III-3b) and (III-6), we have to rely on numerical integration.

Practical applications and experiences suggested that energy for the desired signal and the interfering signal has to be integrated over the directional sectors, respectively, instead of delta functions for single rays. Hence, we write

$$P_I(k, \phi_o) = \int_{\phi_I - \delta_I}^{\phi_I + \delta_I} P(k, \phi, \phi_o)\, d\phi \qquad \text{(III-7b)}$$

where ϕ_I is the azimuth of energy interfering with the signal, and, δ_I is the integration range for interfering energy, and

$$P_S(k, \phi_o) = \int_{\phi_o - \delta_S}^{\phi_o + \delta_S} P(k, \phi, \phi_o)\, d\phi \qquad \text{(III-7c)}$$

for the power of the signal being enhanced where ϕ_o was defined before as the azimuth for the desired signal and δ_S is its integration range. Finally, the total energy $E(k, \phi_o)$ being received by the array is

$$E(k, \phi_o) = P_N(k, \phi_o) + g_S P_S(k, \phi_o) + g_I P_I(k, \phi_o) \qquad \text{(III-8)}$$

where g_S and g_I are the positive scaling parameters for the two mixed signals. We note that there is no distribution function (in terms of azimuths) applied in the integrations of equations (III-7). We assume that signal intensity is equally distributed over the azimuthal space for the integration range of interest.

c. Minimization of Array Power Response

In order to design coefficients which enhance the desired signal and reduces the interfering energy, the array power response, $E'(k, \phi_o)$ must be written as

$$E'(k, \phi_o) = P_N(k, \phi_o) - g_S P_S(k, \phi_o) + g_I P_I(k, \phi_o) \quad . \qquad \text{(III-9)}$$

We used the variational principle with respect to the parameters a_j, where $j = 1, 2, \ldots, N$, so that we minimize the power response such that

$$\frac{\partial E'(k, \phi_o)}{\partial a_j} = 0 \qquad j = 1, 2, \ldots, N \, . \qquad \text{(III-10)}$$

Recall that $E'(k, \phi_o)$ is a function of array coefficients a as indicated in equation (III-3b). Equation (III-10) has a trivial solution which is of no interest. To avoid it, we imposed a constraint condition on the filter weights

$$\sum_{j=1}^{N} a_j = 1 \, . \qquad \text{(III-11)}$$

The constraints in equation (III-11) also preserve the filter weights to have a unity response in array beam direction ϕ_o.

The solution for equation (III-10), along with the constraints of equation (III-11) can be obtained by Lagrange's multiplier method in which we write

$$L = E'(k, \phi_o) + \xi \left(\sum_{j=1}^{N} a_j - 1 \right) \, . \qquad \text{(III-12)}$$

Hence, the variational principle becomes

$$\frac{\partial L}{\partial a_j} = 0, \qquad j = 1, 2, \ldots, N \tag{III-31a}$$

and

$$\frac{\partial L}{\partial \xi} = 0 . \tag{III-13b}$$

The set of equations (III-13a) (III-13b) is an N+1 simultaneous equation and their matrix form is

$$\begin{bmatrix} R_{1\,1} & R_{1\,2} & R_{1\,3} \cdots\cdots R_{1\,N} & 1 \\ R_{2\,1} & R_{2\,2} & R_{2\,3} \cdots\cdots R_{2\,N} & 1 \\ R_{3\,1} & R_{3\,2} & R_{3\,3} \cdots\cdots R_{3\,N} & 1 \\ \vdots & \vdots & \vdots \qquad\qquad \vdots & \vdots \\ R_{N\,1} & R_{N\,2} & \cdots\cdots\cdots R_{N\,N} & 1 \\ 1 & 1 & 1 \cdots\cdots\cdots 1 & 0 \end{bmatrix} \begin{bmatrix} a_1 \\ a_2 \\ \vdots \\ a_N \\ \xi \end{bmatrix} = \begin{bmatrix} 0 \\ \vdots \\ 1 \end{bmatrix} \tag{III-14}$$

where

$$R_{\ell\, j} = \int_0^{2\pi} C_{\ell\, j}\, d\phi - g_S \int_{\phi_o - \delta_S}^{\phi_o + \delta_S} C_{\ell\, j}\, d\phi + g_I \int_{\phi_I - \delta_I}^{\phi_I + \delta_I} C_{\ell\, j}\, d\phi . \tag{III-15}$$

$C_{\ell\, j}$ is referred to equation (III-6) and we note: $C_{\ell\, j} = 1$ when $\ell = j$.

2. Complex Amplitude Weighting Algorithm

In a straightforward manner, equation (III-1) can be multiplied by a complex number to achieve the shading purpose for both amplitudes and

phases. Let's write

$$a_j = a_j^R + i a_j^{IM} \tag{III-16}$$

where $j = 1, 2, \ldots, N$, for the filter weights. We immediately realized that a_j^{IM} was zero and all filter weights were zero-phased in the case of a real amplitude shading algorithm. The power for a single ray of waves received by the array is

$$P(k, \phi, \phi_o) = \sum_{\ell=1}^{N} \sum_{j=1}^{N} a_j a_\ell^* e^{i\left[k(x_j - x_\ell)(\sin\phi - \sin\phi_o) + k(y_j - y_\ell)(\cos\phi - \cos\phi_o)\right]} \tag{III-17}$$

or

$$P(k, \phi, \phi_o) = \sum_{j=1}^{N} (a_j^R)^2 + (a_j^{IM})^2$$

$$+ 2 \sum_{j > \ell} \sum \left[(a_\ell^R a_j^R + a_\ell^{IM} a_j^{IM}) \cos(ARG_{\ell j}) \right.$$

$$\left. - (a_\ell^{IM} a_j^R - a_\ell^R a_j^{IM}) \sin(ARG_{\ell j}) \right] \tag{III-18}$$

where the argument ARG is

$$ARG_{\ell j} = k(x_j - x_\ell)(\sin\phi - \sin\phi_o) + k(y_j - y_\ell)(\cos\phi - \cos\phi_o) . \tag{III-19}$$

We would use the same physical model described before for the formulation and accordingly would obtain the same generalized form of equation (III-9) for the array power response. Following the same variational principle of minimizing the power response with respect to filter weights,

we required that

$$\frac{\partial E'(k, \phi_o)}{\partial a_j^R} = 0 \qquad \text{(III-20)}$$

and

$$\frac{\partial E'(k, \phi_o)}{\partial a_j^{IM}} = 0 \qquad \text{(III-21)}$$

where $j = 1, 2, \ldots, N$. To avoid the trivial solution where $a_j^R = 0$ and $a_j^{IM} = 0$, it is required to impose the constraints on the filter weights. Without getting into the trouble of solving the second order simultaneous equations, the following simple constraints are introduced:

$$\begin{cases} \sum_{j=1}^{N} a_j^R = 1 \\ \sum_{j=1}^{N} a_j^{IM} = 1 \end{cases} \qquad \text{(III-22)}$$

or

$$\begin{cases} \sum_{j=1}^{N} a_j^R = 1 \\ \sum_{j=1}^{N} a_j^{IM} = 0 \end{cases} . \qquad \text{(III-23)}$$

We will show in Subsection III-C that the constraints in equations (III-22) and (III-23) yield different solutions of filter weights, but result in the same power response pattern.

We would use the Lagrange's multiplier method again for obtaining the optimum solution. Let's write the Lagrangian, $\Phi(k)$ in this case such that

$$\Phi(k) = E'(k, \phi_o) + \xi\left(\sum_{j=1}^{N} a_j^R - 1\right) + \eta\left(\sum_{j=1}^{N} a_j^{IM} - 1\right) \qquad \text{(III-24)}$$

for the constraints of equation (III-22), and

$$\Phi'(k) = E'(k, \phi_o) + \xi\left(\sum_{j=1}^{N} a_j^R - 1\right) + \eta\left(\sum_{j=1}^{N} a_j^{IM}\right) \qquad \text{(III-25)}$$

for the constraints of equation (III-23). Then the variational principle states

$$\frac{\partial \Phi(k)}{\partial a_j^R} = 0 \qquad \text{(III-26a)}$$

$$\frac{\partial \Phi(k)}{\partial a_j^{IM}} = 0 \qquad \text{(III-26b)}$$

$$\frac{\partial \Phi(k)}{\partial \xi} = 0 \qquad \text{(III-26c)}$$

and

$$\frac{\partial \Phi(k)}{\partial \eta} = 0 \qquad \text{(III-26d)}$$

where $j = 1, 2, \ldots, N$ and where N is the number of sensors in the array. There are $2N+2$ simultaneous equations to solve for $2N+2$ unknown variables.

The matrix form for equation (III-26) is written here:

$$\begin{bmatrix} T_{11} & T_{12} & T_{13}\cdots T_{1N} & S_{11} & S_{12} & S_{13}\cdots S_{1N} & 1 & 0 \\ T_{21} & T_{22} & T_{23}\cdots T_{2N} & S_{21} & S_{22} & S_{23}\cdots & 1 & 0 \\ T_{31} & T_{32} & T_{33}\cdots & S_{31} & S_{32} & S_{33}\cdots & \vdots & \vdots \\ \vdots & \vdots & \vdots & \vdots & \vdots & \vdots & \vdots & \vdots \\ T_{N1} & T_{N2} & \cdots T_{NN} & S_{N1} & \cdots & S_{NN} & 1 & 0 \\ S_{11} & S_{21} & S_{31}\cdots S_{N1} & T_{11} & T_{12} & T_{13}\cdots T_{1N} & 0 & 1 \\ S_{12} & S_{22} & S_{31}\cdots & T_{21} & T_{22} & T_{23}\cdots & 0 & 1 \\ S_{13} & S_{23} & \vdots & T_{31} & T_{32} & T_{33} & \vdots & \vdots \\ \vdots & \vdots & \vdots & \vdots & \vdots & \vdots & \vdots & \vdots \\ S_{1N} & \cdots & S_{NN} & T_{N1} & \cdots & T_{NN} & 0 & 1 \\ 1 & 1\cdots & 1 & 0 & 0\cdots & 0 & 0 & 0 \\ 0 & 0\cdots & 0 & 1 & 1\cdots & 1 & 0 & 0 \end{bmatrix} \begin{bmatrix} a_1^R \\ a_2^R \\ \vdots \\ a_N^R \\ a_1^{IM} \\ a_2^{IM} \\ \vdots \\ a_N^{IM} \\ \xi \\ \eta \end{bmatrix} = \begin{bmatrix} 0 \\ 0 \\ \vdots \\ 0 \\ 1 \\ 1 \end{bmatrix} \qquad \text{(III-27)}$$

where

$$T_{\ell j} = \int_0^{2\pi} \cos(ARG_{\ell j})d\phi - g_S \int_{\phi_o-\delta_S}^{\phi_o+\delta_S} \cos(ARG_{\ell j})d\phi + g_I \int_{\phi_I-\delta_I}^{\phi_I+\delta_I} \cos(ARG_{\ell j})d\phi \qquad \text{(III-28)}$$

and

$$S_{\ell j} = \int_0^{2\pi} \sin(ARG_{\ell j})d\phi - g_S \int_{\phi_o-\delta_S}^{\phi_o+\delta_S} \sin(ARG_{\ell j})d\phi + g_I \int_{\phi_I-\delta_I}^{\phi_I+\delta_I} \sin(ARG_{\ell j})d\phi \qquad \text{(III-29)}$$

where $ARG_{\ell j}$ was defined in equation (III-19). We note that $ARG_{\ell j} = 0$ if

$\ell = j$, $T_{\ell j} = T_{j\ell}$, and $S_{\ell j} = -S_{j\ell}$. For the constraints of equation (III-23), the right-hand side of matrix equation (III-27) would be

$$\begin{bmatrix} 0 \\ 0 \\ \vdots \\ 0 \\ 1 \\ 0 \end{bmatrix}.$$

C. THEORETICALLY CALCULATED ARRAY RESPONSE PATTERNS

Computation for both the real and complex amplitude weighting algorithms was done on an IBM 360/44 computer for various physical design parameters defined before. Presented here are only the related examples which were applied in the test using the recorded data from the KSRS short-period seismic array. Table III-1 shows the relative locations of seismic sensors in the array.

Figure III-1 shows the computed power response pattern for the beamsteer (time-alignment and average) processor. The array was steered at the 290° azimuth, the wave frequency was 2.0 Hz; and the phase velocity was 14.3 km/sec. Velocity and azimuth of a seismic bodywave as viewed by sensors in a given array indicated the location of a seismic source in the earth. In this case, the corresponding signal source was in Tadzhik, USSR.

Figure III-2 shows the computed power response pattern for the real-amplitude-weighted array. The input parameters are:

f = 2.0 Hz

v = 14.3 km/sec

TABLE III-1

RELATIVE LOCATIONS OF KOREAN SEISMIC RESEARCH STATIONS SHORT-PERIOD ARRAY SENSORS (POSITIVE Y-AXIS IS POINTING TO THE NORTH, WHILE POSITIVE X TO THE EAST)

Sensors	X (km)	Y (km)
1	0.0	0.0
2	0.79	2.11
3	2.08	0.13
4	2.29	-2.25
5	-0.19	-2.13
6	-1.98	-0.63
7	-1.90	1.24
8	-0.51	4.28
9	2.47	3.76
10	3.20	2.10
11	5.24	0.36
12	4.27	-1.39
13	3.15	-3.49
14	1.26	-4.81
15	-0.91	-3.81
16	-3.46	-2.71
17	-4.76	-0.95
18	-4.41	1.09
19	-2.38	2.87

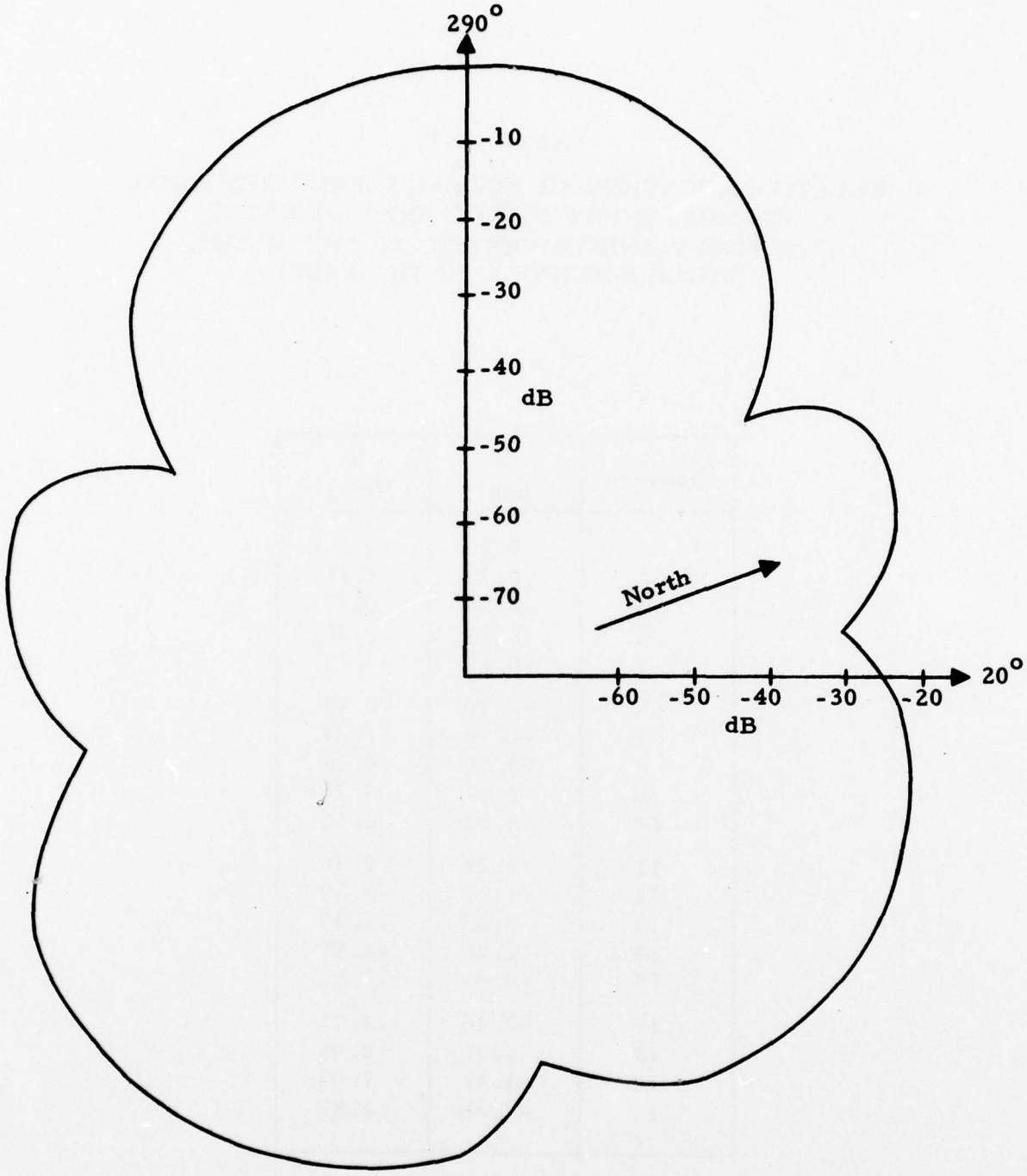

FIGURE III-1

COMPUTED BEAMSTEER RESPONSE PATTERN FOR
2.0 Hz AND 14.3 km/sec WAVE

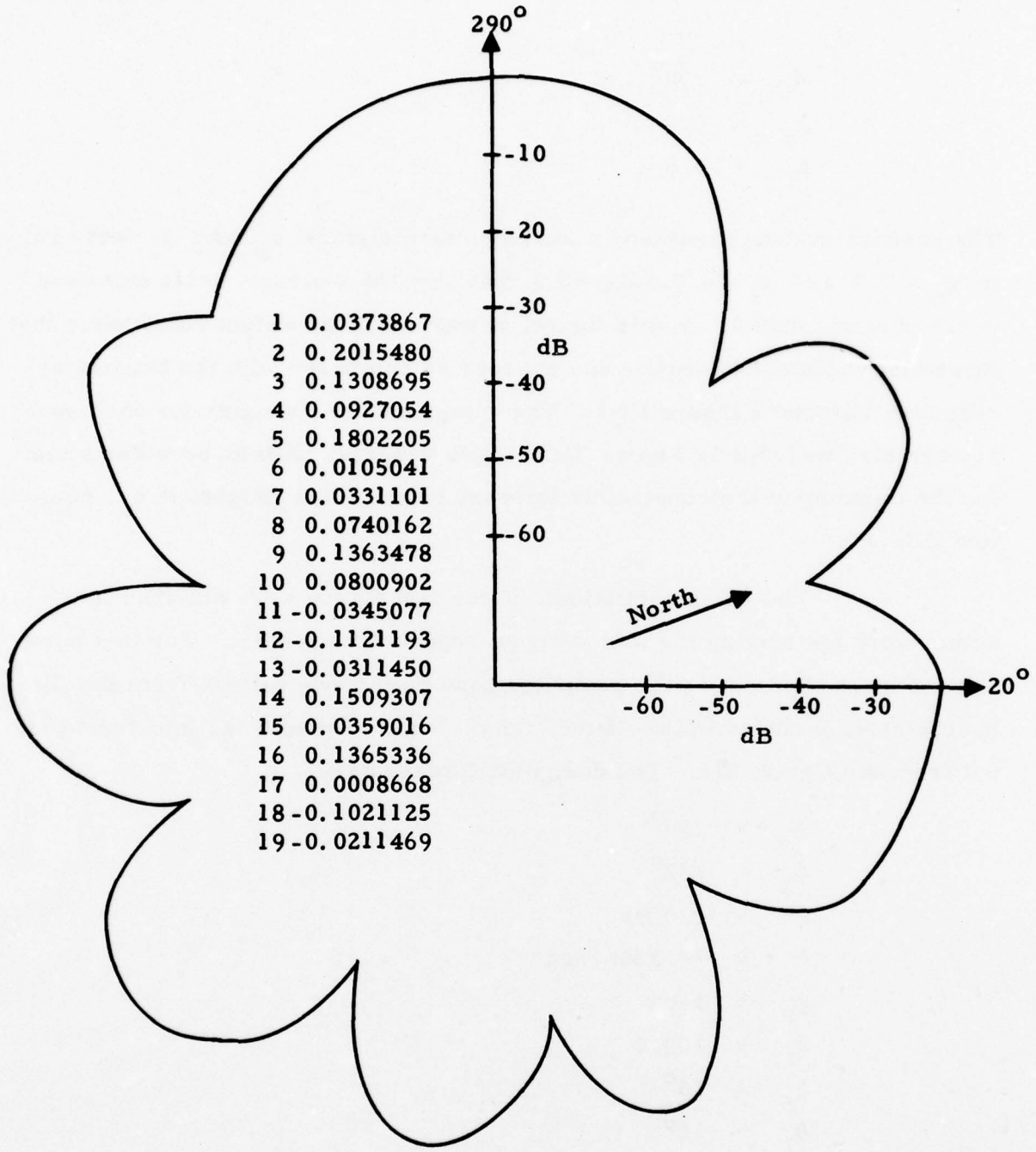

FIGURE III-2

COMPUTED POWER RESPONSE PATTERN FOR REAL-AMPLITUDE-SHADED ARRAY (f = 2.0 Hz, v = 14.3 km/sec, g_S = 0.0, g_I = 0.0)

$$\phi_o = 290^o$$
$$g_S = 0.0$$
$$g_I = 0.0 \ .$$

The positive scaling parameters for two mixed signals g_S and g_I were set to $g_S = 0.0$ and $g_I = 0.0$, suggesting that only the isotropic noise was used in the physical model. In this figure, it was the filter weight constraints that forced the mainlobe narrower and sharper as compared with the beamsteer response pattern in Figure III-1. The computed filter weights for each sensor are also included in Figure III-2. This response pattern provides a test for the meaning of the constraints imposed on the filter weights (i.e., equation (III-11)).

The filter coefficients in the last figure were not used in the actual work for solving the mixed signal separation problem. For that purpose, Figure III-3 shows the computed power response pattern from the filter coefficients, included in the figure, for the suppression of the interfering signal from the Ceram Sea. The design parameters are:

$$\phi_o = 290^o$$
$$\phi_I = 182^o$$
$$f = 2.0 \text{ Hz}$$
$$v = 14.3 \text{ km/sec}$$
$$g_S = 1.0$$
$$g_I = 100.0$$
$$\delta_S = 15^o$$
$$\delta_I = 15^o \ .$$

In this case, the 182^o null steering azimuth was intended to reduce the interfering signal from a strong earthquake in Ceram, Indonesia.

A complex amplitude weighting algorithm was also programmed for computation and tested with the recorded data. Figure III-4 shows the

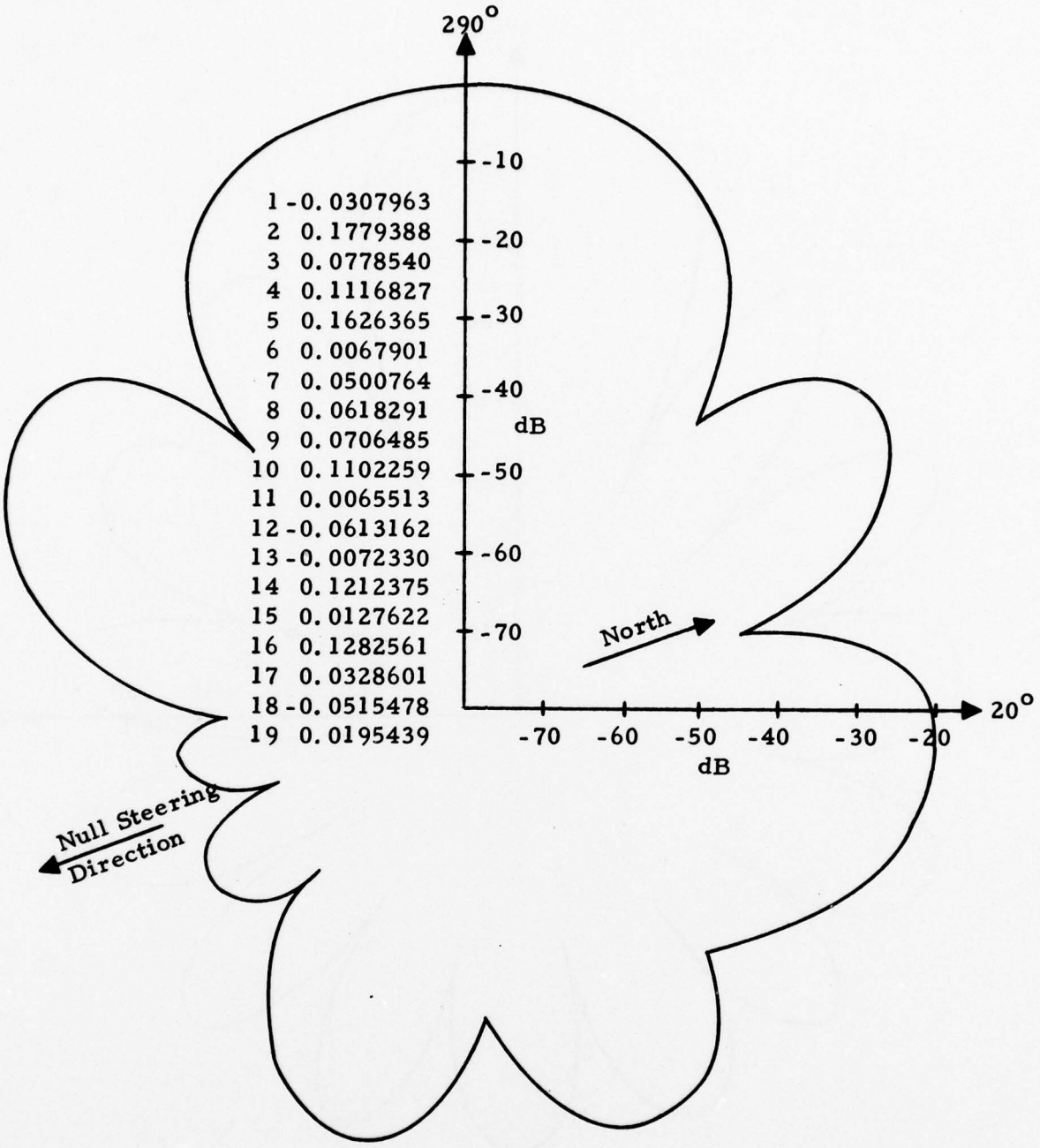

FIGURE III-3

COMPUTED POWER RESPONSE PATTERN FOR REAL-AMPLITUDE-SHADED ARRAY FOR INTERFERING SIGNAL AT 182° AZIMUTH
(f = 2.0 Hz, v = 14.3 km/sec, g_S= 1.0, g_I= 100.0, δ_S= 15°, AND δ_I= 15°)

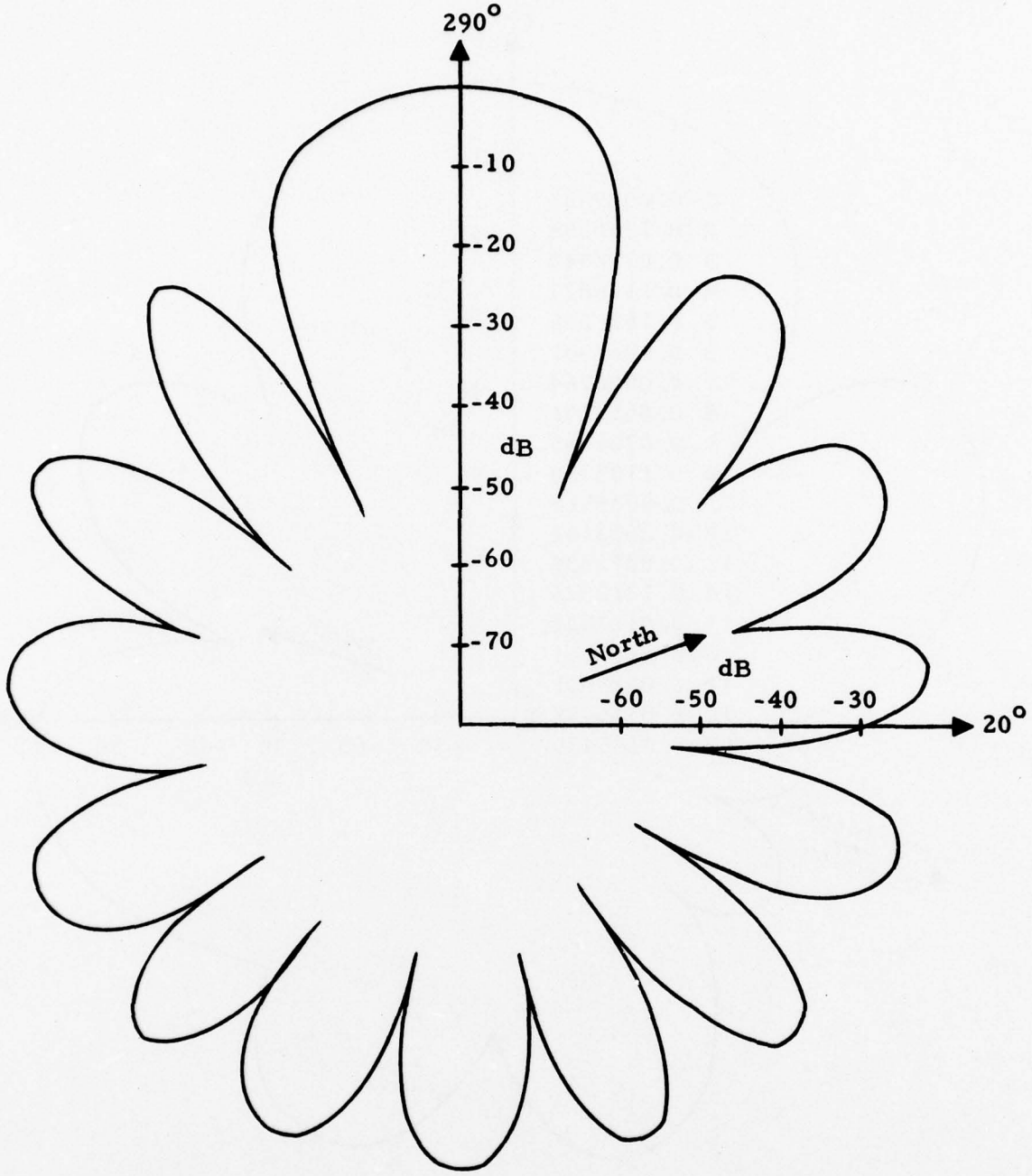

FIGURE III-4

COMPUTED POWER RESPONSE PATTERN FOR COMPLEX FILTER WEIGHTS IN TABLE III-2 (f = 2.0 Hz, v = 14.3 km/sec, g_S = 0.0, AND g_I = 0.0)

computed power response pattern for the physical model of isotropic noise only. The parameters used are:

$f = 2.0$ Hz

$v = 14.3$ km/sec

$\phi_o = 290^o$

$g_S = 0.0$

$g_I = 0.0$.

The corresponding computed filter weights were listed in Table III-2 where (a) was for the constraints in equation (III-22) and (b) for the constraints in equation (III-23). The two constraint conditions yielded the same response pattern in Figure III-4 but different filter weights. The test in this case provided no actual application, but a practical realization for the filter weight constraints used in the algorithm.

To demonstrate the null steering capability for the algorithm, Figure III-5 shows the computed power response pattern for the complex-shaded array. The corresponding computed complex filter weights for the two constraint conditions were listed in Table III-3. The input parameters for the computation are:

$f = 2.0$ Hz

$v = 14.3$ km/sec

$\phi_o = 290^o$

$\phi_I = 182^o$

$g_S = 1.0$

$g_I = 125.0$

$\delta_S = 9^o$

$\delta_I = 12^o$.

The two constraint conditions yielded the different sets of filter weights, but resulted in the same power response pattern as mentioned earlier.

TABLE III-2

COMPLEX FILTER WEIGHTS FOR FIGURE III-4

(f = 2.0 Hz, v = 14.3 km/sec, g_S = 0.0, g_I = 0.0)

(a)

Sensor	a^R	a^{IM}
1	-1.3111753	-0.4014696
2	0.5705968	-3.3882036
3	2.4232225	0.6496993
4	1.5117025	2.7724333
5	-2.1410198	-1.3655806
6	1.3891954	2.2052984
7	0.3291515	-6.9080343
8	-0.8699333	-2.3466024
9	0.2080652	3.0515318
10	-3.3849630	1.8806114
11	1.1869287	0.5927187
12	0.9683687	4.5879803
13	-2.2162609	3.0825062
14	-1.9140673	-0.3550996
15	-0.0366499	1.3466063
16	0.0156091	-4.0992146
17	2.3782892	-0.0545951
18	1.7750101	0.5109112
19	0.1179288	-0.7614973
Sum	1.0	1.0

(b)

Sensor	a^R	a^{IM}
1	-0.8563225	0.4548528
2	-1.4088030	-1.9793997
3	1.5364609	-0.8867619
4	2.1420679	0.6303653
5	-1.7533007	0.3877194
6	1.7972469	0.4080514
7	-3.2894411	-3.6185923
8	-1.6082678	-0.7383346
9	1.6297979	1.4217329
10	-0.7521755	2.6327877
11	0.8898240	-0.2971053
12	2.7781744	1.8098059
13	0.4331227	2.6493835
14	-1.1345835	0.7794842
15	0.6549784	0.6916283
16	-2.0418024	-2.0574121
17	1.1618471	-1.2164421
18	1.1429605	-0.6320499
19	-0.3217842	-0.4397131
Sum	1.0	0.0

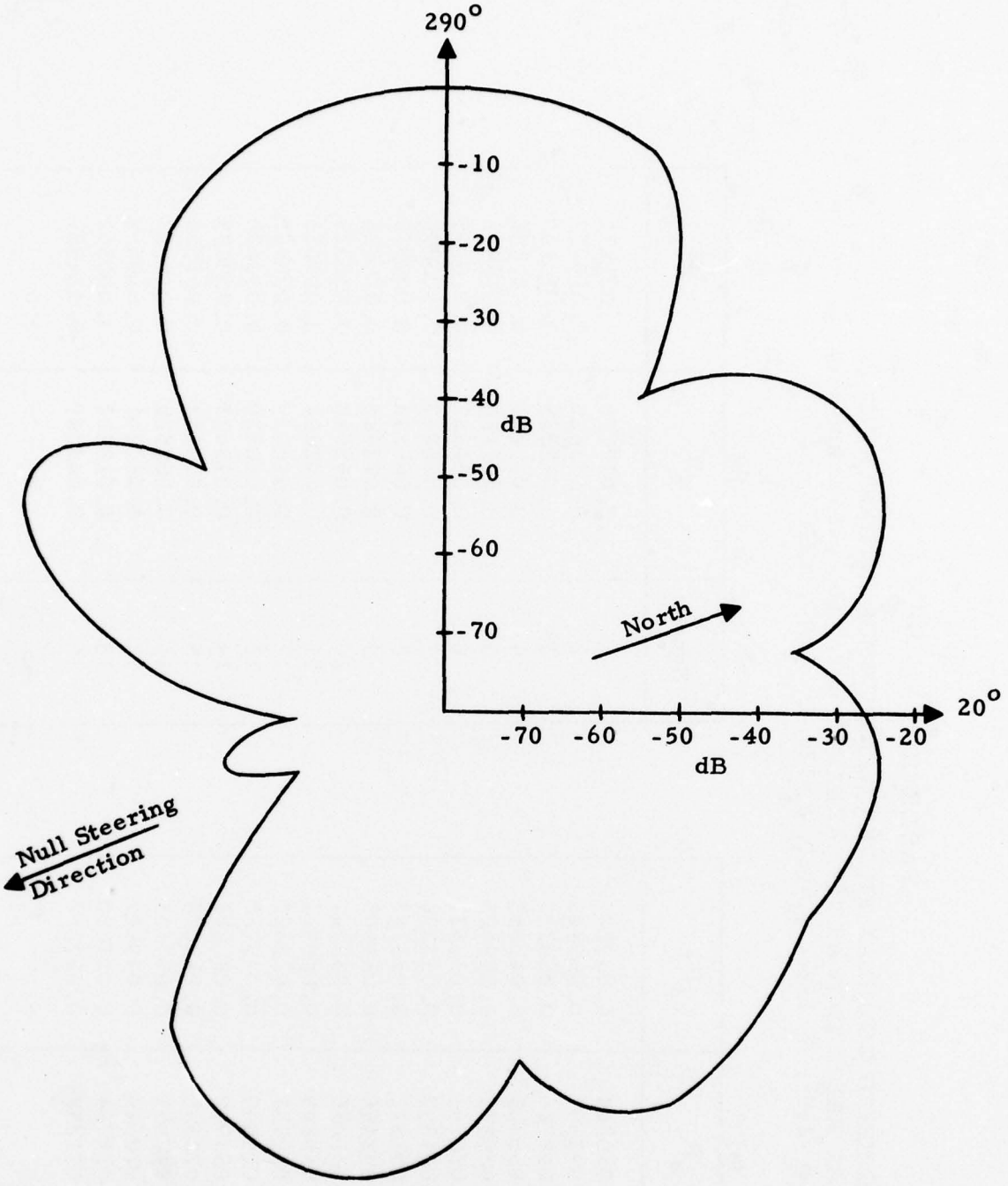

FIGURE III-5

COMPUTED POWER RESPONSE PATTERN FOR COMPLEX SHADED ARRAY WITH FILTER WEIGHTS GIVEN IN TABLE III-3 ($\phi_S = 290^\circ$, $\phi_I = 182^\circ$, $g_S = 1.0$, $g_I = 125$, $\delta_S = 9^\circ$, AND $\delta_I = 12^\circ$)

TABLE III-3

DESIGNED COMPLEX FILTER WEIGHTS FOR INTERFERING SIGNAL REDUCTION AT 182° AZIMUTH (f=2.0 Hz, v=14.3 km/sec, ϕ_o=290°, ϕ_I=182°, g_S=1.0, g_I=125.0, δ_S=9°, AND δ_I=12°)

(a)

Sensor	a^R	a^{IM}
1	0.036344	0.039207
2	0.093397	0.053843
3	0.047786	0.069323
4	0.065303	0.041659
5	0.025277	0.059023
6	0.070767	0.038537
7	0.044597	0.052336
8	0.058571	0.073717
9	0.092455	0.051603
10	0.021256	0.085907
11	0.039809	0.045914
12	0.009731	0.022427
13	0.019899	0.072760
14	0.063940	0.082905
15	0.072586	0.068678
16	0.077651	0.057405
17	0.070640	0.049842
18	0.018754	0.017650
19	0.071237	0.017262
Sum	1.0	1.0

(b)

Sensor	a^R	a^{IM}
1	0.037776	0.001431
2	0.073620	-0.019777
3	0.058555	0.010769
4	0.053481	-0.011822
5	0.042150	0.016873
6	0.054652	-0.016115
7	0.048467	0.003870
8	0.066144	0.007573
9	0.072029	-0.020426
10	0.053582	0.032325
11	0.042861	0.003053
12	0.016079	0.006348
13	0.046329	0.026430
14	0.073423	0.009483
15	0.070632	-0.001954
16	0.067528	-0.010123
17	0.060241	-0.010399
18	0.018202	-0.000552
19	0.044249	-0.026987
Sum	1.0	0.0

D. PRELIMINARY COMMENTS

The power response patterns presented so far were limited to the case of one frequency only. Limited computational experience on various sets of parameters indicated that the real amplitude shading algorithm was more stable than the complex amplitude shading algorithm. The reason is simple: The real-amplitude algorithm requires only N+1 simultaneous equations for an N-channel array, while the complex-amplitude algorithm needs 2N+2 simultaneous equations. The larger matrix inversion yields the poorer accuracy for numerical solutions, and resulted in the less stable system for the algorithm. Also, the present complex shading algorithm needed four times as much computation time as the real amplitude shading algorithm. Examination of the null-steering produced in the azimuth range between 160° and 210° was examined by comparing the maximum lobes within that range. For real coefficients the rejection in that azimuth range was -40 dB; for complex weights, -50 dB. This compares to -16 dB and -24 dB, respectively, for isotropic noise rejection using real and complex weights.

Normally, the solution of filter weights, real or complex, depended on the parameters used; i.e., f, v, g_S, g_I, δ_S, and δ_I. The use of g_S functioned as a directivity design parameter, while g_I as the null-steering parameter which controls the null-response levels. The stability of the solution was highly dependent on the azimuthal separation between the interfering signal and the desired signal, $\phi_o - \phi_I$, and the wavelength of a seismic P wave, λ.

SECTION IV

EXPERIMENTAL RESULTS FROM RECORDED SEISMIC ARRAY DATA

A. DATA

The algorithms were tested using the recorded data from the short-period array at the Korean Seismic Research Station (KSRS). The KSRS short-period array has 19 sensors with an aperture of about 10 km. The configuration consists of two concentric rings: 6 sensors in the inner ring and 12 sensors in the outer ring with one in the center. The relative coordinates of sensors have been presented in Table III-1. The data used in this report were digitized at sampling time interval $\Delta t = 0.1$ seconds.

Two earthquake events were used for mixed-signal data: one was from Ceram Sea, Indonesia (NEIS: 01/01/77, 19.01.40, 2.532S, 126.582 E, $m_b = 6.0$) and the other from Tadzhik, USSR (NEIS: 03/08/77, 15.28.47, 38.03N, 69.44E, $m_b = 5.2$). The first event had a very strong and long wavetrain recorded at KSRS and was used as the strong interfering signal. The second event had signal amplitude at the noise level and was undetectable in the single sensor data, but detectable in the array beam.

To demonstrate the performance of techniques we developed for the mixed-signal situations, the raw data of the weaker signal were added to those of the much stronger signal. Figure IV-1 shows the composite data (in 0.5 - 3.5 Hz passband) which simulated the recorded mixed signal situations. In this case, the raw data of the stronger signal had been scaled by a factor of 0.1 before they were added to the data of the weaker signal. The signal wavetrains from Ceram Sea dominate the display, while the later arriving signal from Tadzhik is hidden by the visible wavetrains of the Ceram Sea event about 33 seconds after its first arrival.

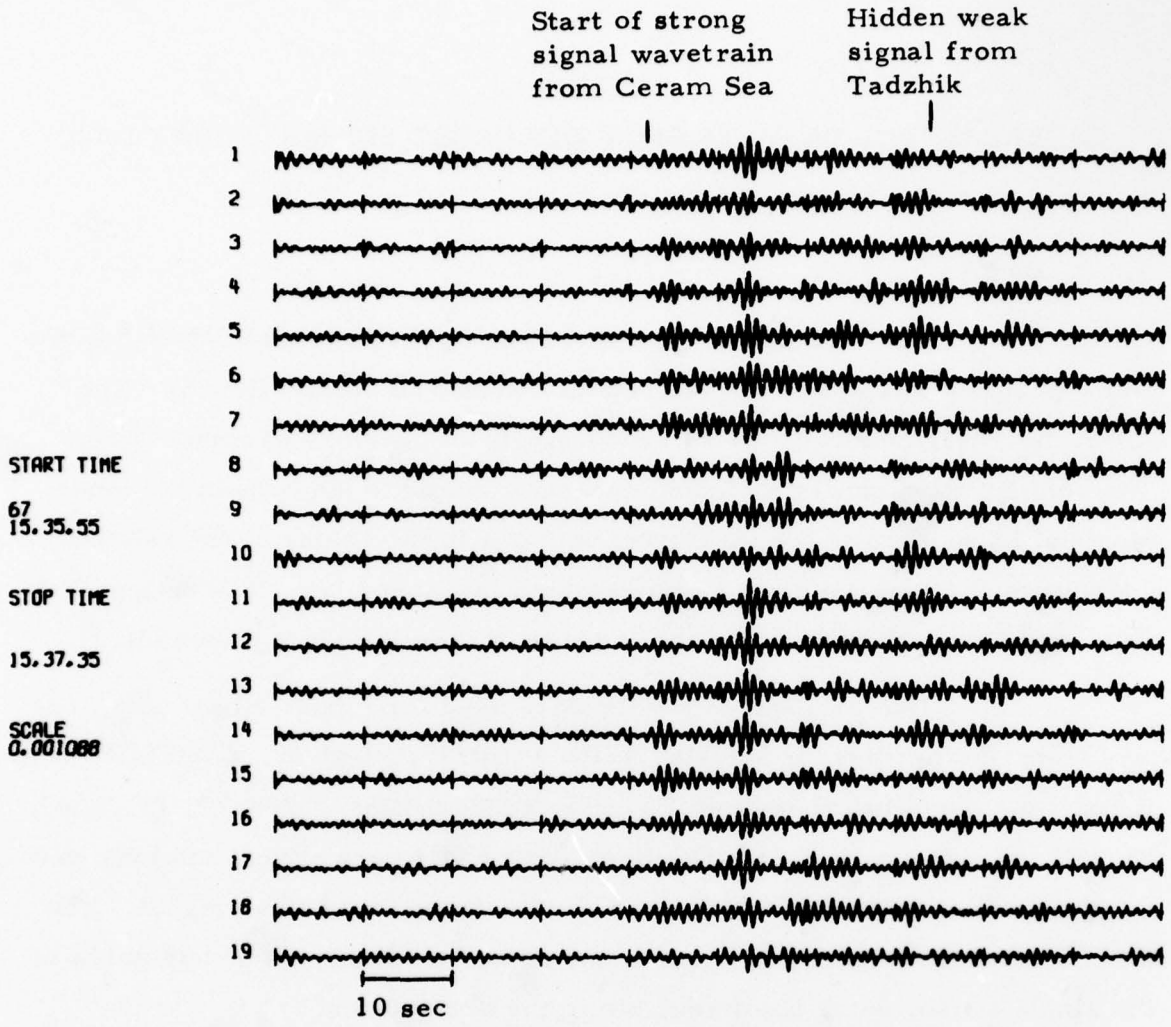

FIGURE IV-1

COMPOSITE DATA OF MIXED SIGNALS
(0.5-3.5 Hz)

Figure IV-2 displays the same mixed signal data in the 1.5 - 2.5 Hz passband.

B. ADAPTIVE BEAMFORMING OUTPUTS

The composite data which simulated the recorded short-period data at KSRS for mixed signal situations were first processed by the adaptive beamformer in various passbands. To display the wavetrains for the signal from the Ceram Sea, we processed the composite data by beamforming the array using the exact location of the stronger signal source. Time-varying adaptation parameters used in this report were $\alpha = 0.0045$, and $\beta = 0.65$ which were found to have optimum SNR for the initial P-wave. Figure IV-3 shows the beamforming outputs (0.5-3.5 Hz) of the composite data by steering the array at the Ceram Sea event. Because the signal amplitude from Ceram was much larger than that from Tadzhik, beamforming of the stronger signal would eliminate the weaker signal. Therefore, the Tadzhik signal disappeared from the array beams in this case.

To demonstrate the weak signal extraction by suppressing the stronger interfering signal in the mixed-signal situation, Figure IV-4 shows the beamforming outputs in the 0.5-1.5 Hz passband of the composite data where the mixed-signal situation is simulated. The array was steered at the Tadzhik location (289° and 14.3 km/sec). The first pulse of wavetrains on the ABF output is the initial arrival of the signal from the Ceram Sea. The signal from Tadzhik was placed 33 seconds after the initial pulse of the Ceram wavetrains as shown on the ABF beams. The figure does show some kind of capability that the adaptive filter removes the interfering coda and successfully separates the mixed-signals. It is noted that a higher μ design of the ABF would totally eliminate the Ceram wavetrains, but it also degraded the Tadzhik signal in this case.

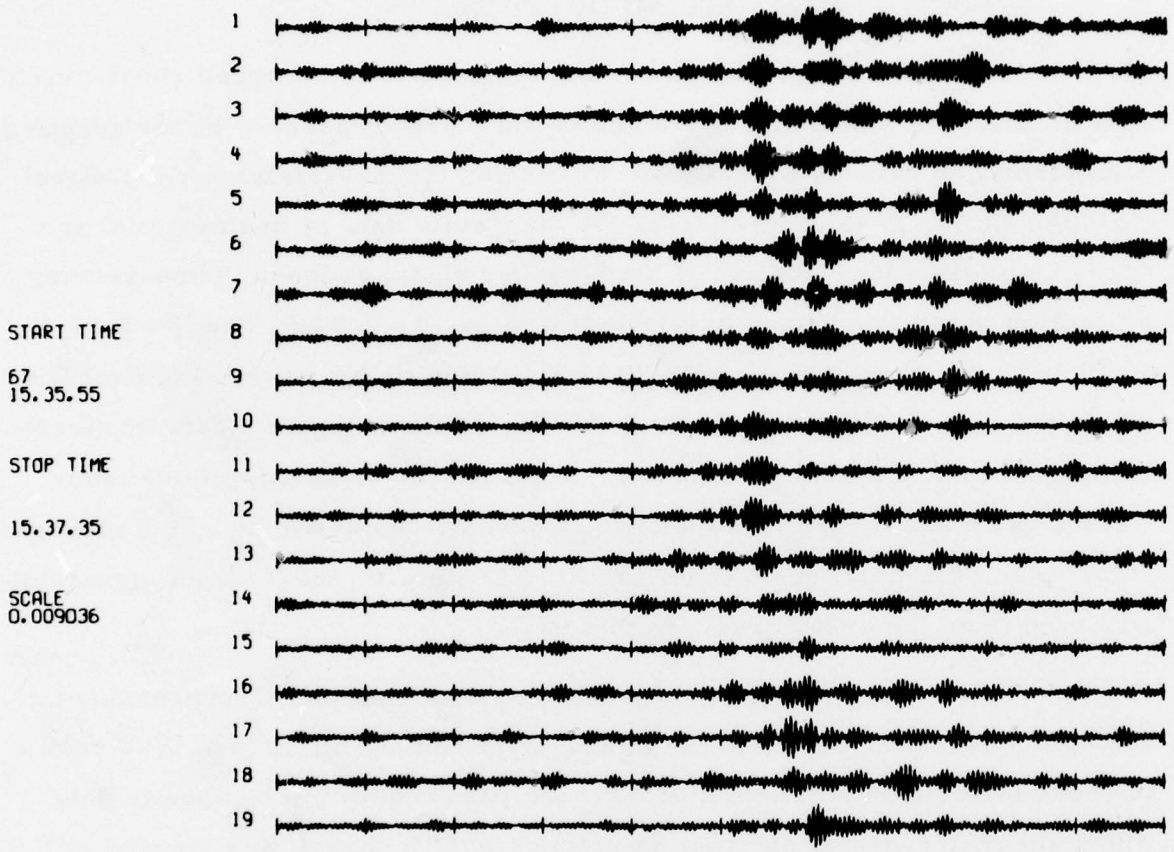

FIGURE IV-2

COMPOSITE DATA OF MIXED SIGNALS
(1.5-2.5 Hz)

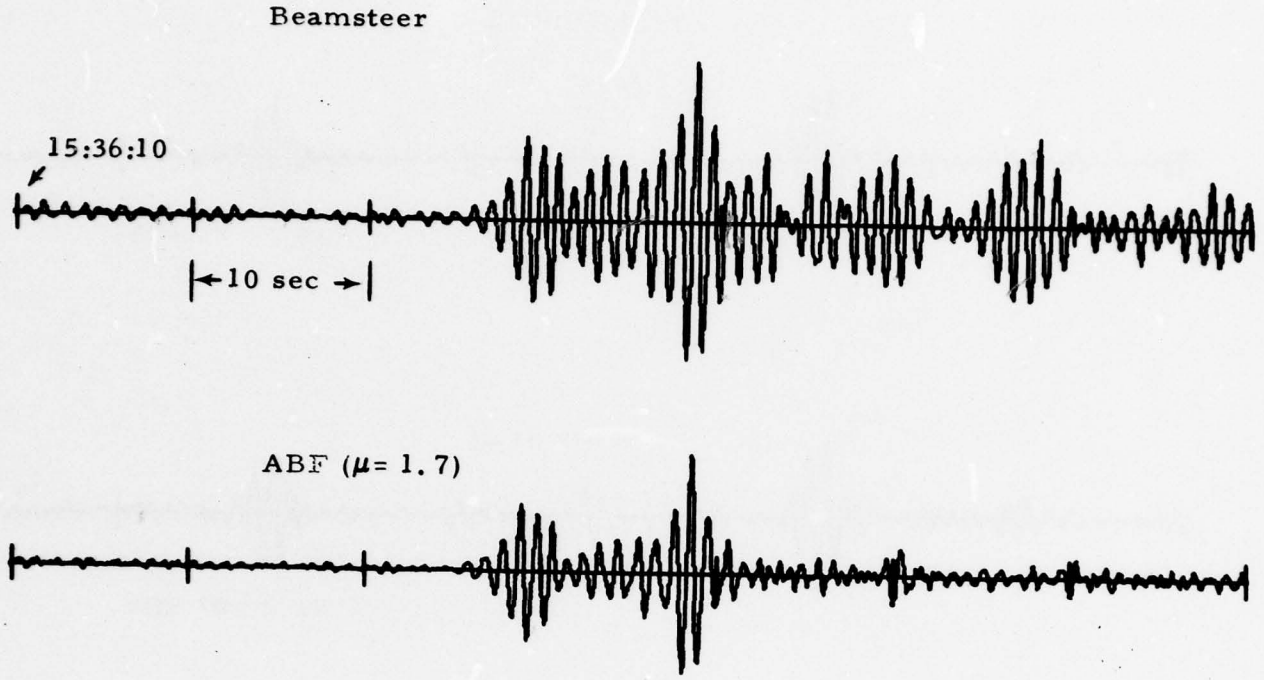

FIGURE IV-3

BEAMFORMING OUTPUTS OF THE MIXED-SIGNAL DATA BY STEERING ARRAY AT CERAM SEA, INDONESIA (0.5-3.5 Hz)

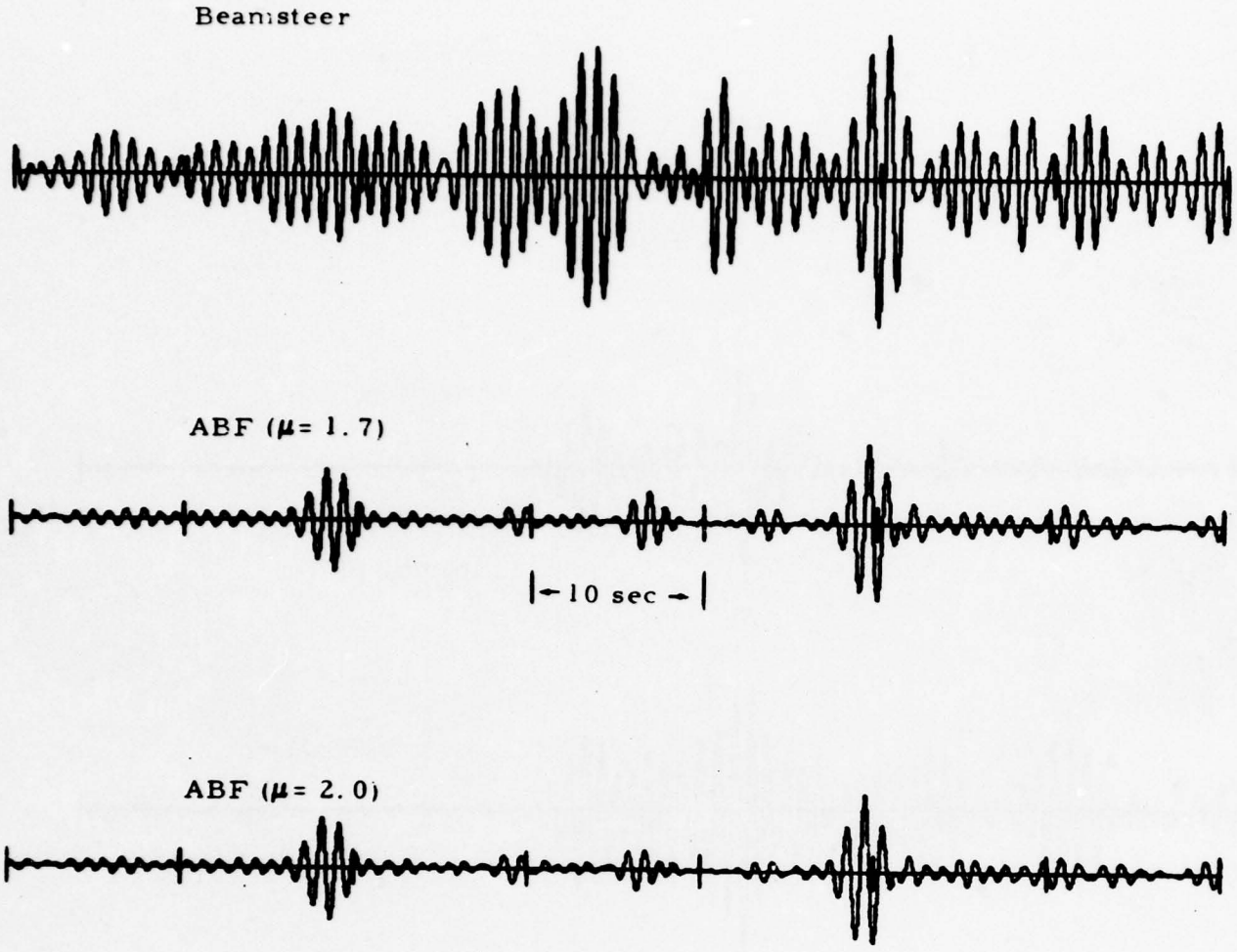

FIGURE IV-4

BEAMFORMING OUTPUTS OF THE MIXED-SIGNAL DATA BY STEERING ARRAY AT TADZHIK, USSR (0.5-1.5 Hz)

Figure IV-5 shows the beamforming output in the 1.5-2.5 Hz band of the composite data. Elimination of strong interfering coda to extract a weaker signal is achieved by the ABF processor in this case.

The last two figures demonstrate mixed-signal separation capability in relatively narrow band cases. For operational purposes, one would like to have a processor to achieve the optimum performance with relative statistical reliability. In that sense, a wider band to cover the most part of the energy for the signals of interest must be chosen. Figure IV-6 shows the beamforming output in the 0.5-3.5 Hz passband for the mixed-signal data. The high amplitude coda generated from the Ceram Sea earthquake was suppressed closer to noise level on the ABF beams. The energy from Tadzhik earthquake was remarkably passed through the ABF processor without degradation. However, it is noted that a lower μ was used in this case.

C. OPTIMUM-SHADED ARRAY BEAMS

The computed filter weights from real-amplitude shading algorithms and from the complex-amplitude algorithm for null-steering were also applied to the mixed-signal data for array beamforming. The array shading algorithms were formulated through the variational principle in the frequency domain for a single frequency. Accordingly, beamforming of array data was done in the frequency domain and the preliminary test of recorded data in this report was limited to narrowband signal wavetrains.

Bandpass filtering was applied to each single channel data in the frequency domain. The bandpass filter applied was

$$H(f) = \tfrac{1}{2}\left[1 + \cos\left(\frac{\pi|f_c - f|}{\Delta f}\right)\right] \qquad \text{for } |f_c - f| \le \Delta f$$

$$= 0 \qquad \text{for } |f_c - f| \ge \Delta f \qquad \text{(IV-1)}$$

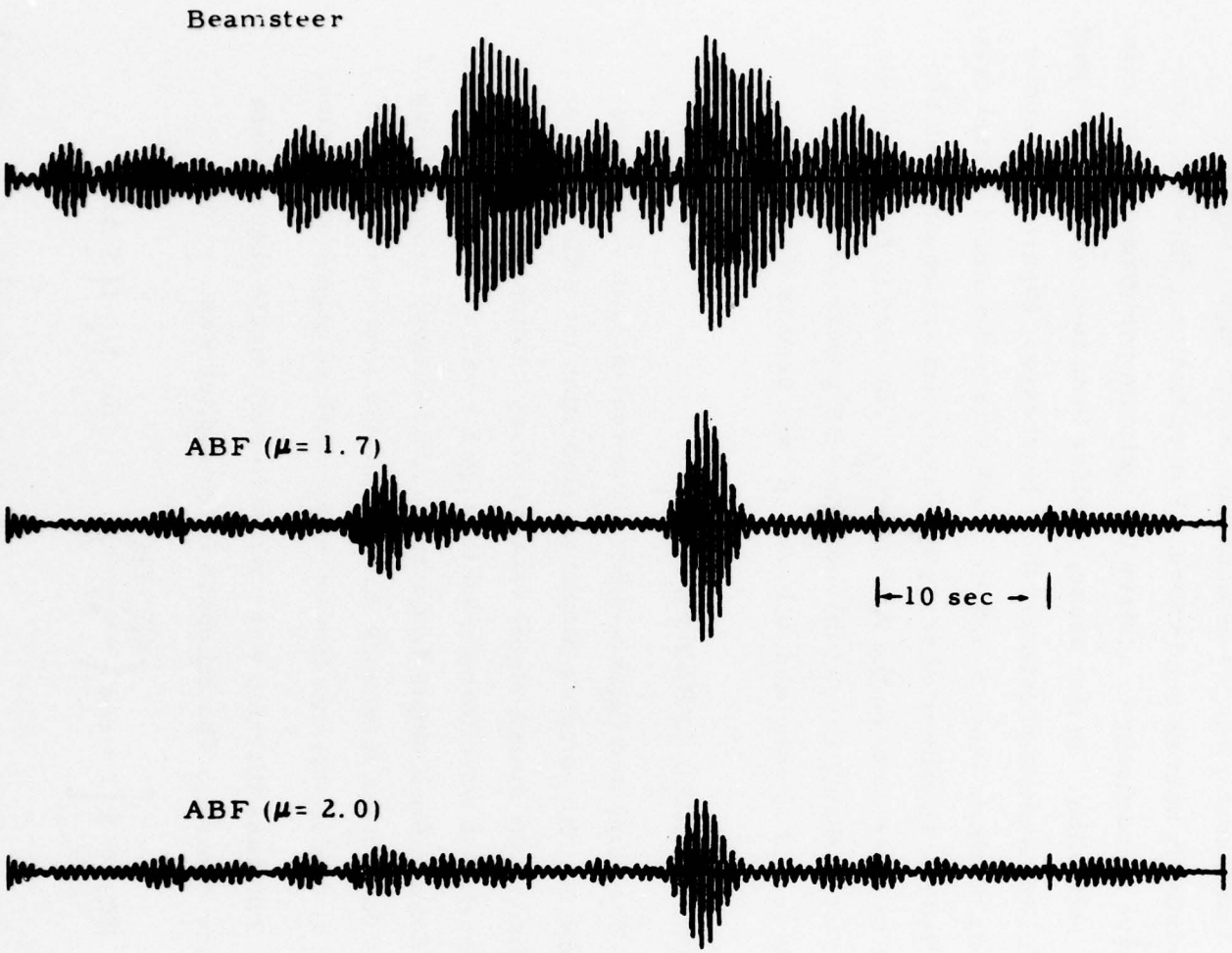

FIGURE IV-5

BEAMFORMING OUTPUTS OF THE MIXED-SIGNAL DATA BY STEERING ARRAY AT TADZHIK, USSR (1.5-2.5 Hz)

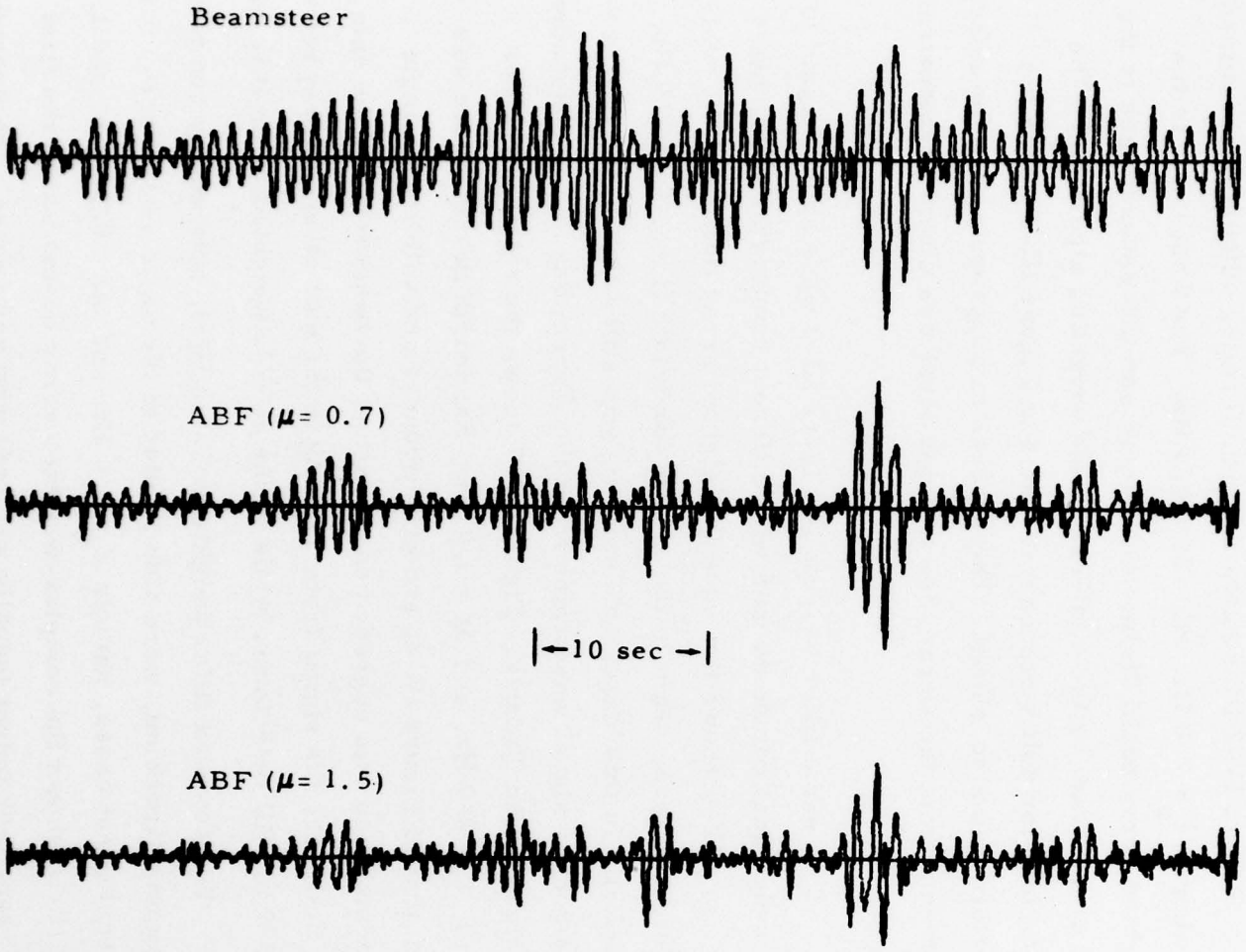

FIGURE IV-6

BEAMFORMING OUTPUTS OF THE MIXED-SIGNAL DATA BY STEERING ARRAY AT TADZHIK, USSR (0.5-3.5 Hz)

where f_c is the carrier frequency and Δf is one half of a bandwidth. Various bandwidths of data were tested to evaluate the effectiveness of single frequency formulation.

Figure IV-7 illustrates the beamforming outputs of the mixed-signal data where $f_c = 2.0$ Hz, and $\Delta f = 0.3$ Hz. The first trace is the equally weighted array beam (beamsteer output) and the second trace is the null steered array beam by the real-amplitude weighting algorithm. The filter weights used for null steering was listed in Figure III-3 where the response pattern was also shown. The success in suppressing the 'interfering' signal wavetrains from the Ceram Sea to noise level was clearly demonstrated in the figure.

The same filter weights in Figure III-3 were applied again to the same mixed-signal composte data with different bandwidths in bandpass filtering. Figure IV-8 shows the equally weighted array beam and the real-amplitude weighted array beam in the 1.0 Hz bandwidth (i.e., $f_c = 2.0$ Hz, and $\Delta f = 0.5$ Hz). In this case, null steering was still very effective in removing the stronger signal wavetrains from the Ceram Sea and in enhancing the weaker signal from Tadzhik. Figure IV-9 shows the relatively wider band data with $f_c = 2.0$ Hz, and $\Delta f = 1.0$ Hz. Bandwidth in this figure was doubled from that of Figure IV-8, and effectiveness and validity of single frequency formulation was degraded somewhat as the bandwidths of the data increased. However, the signal from Tadzhik in the null steered array beam in Figure IV-9 is still detectable, while in the equally weighted beam it is not.

The complex filter weights in Table III-3, obtained by complex-amplitude shading algorithm, were also applied to the same sets of array data for various equivalent cases, namely $f_c = 2.0$ Hz, and $\Delta f = 0.3$, 0.5, and 1.0 Hz. Figure IV-10 shows the complex-weighted array beams where the first trace is the beamsteer output (equally weighted with zero phase), the second trace is the null-steered beam with filter weights in set (a) of Table III-3;

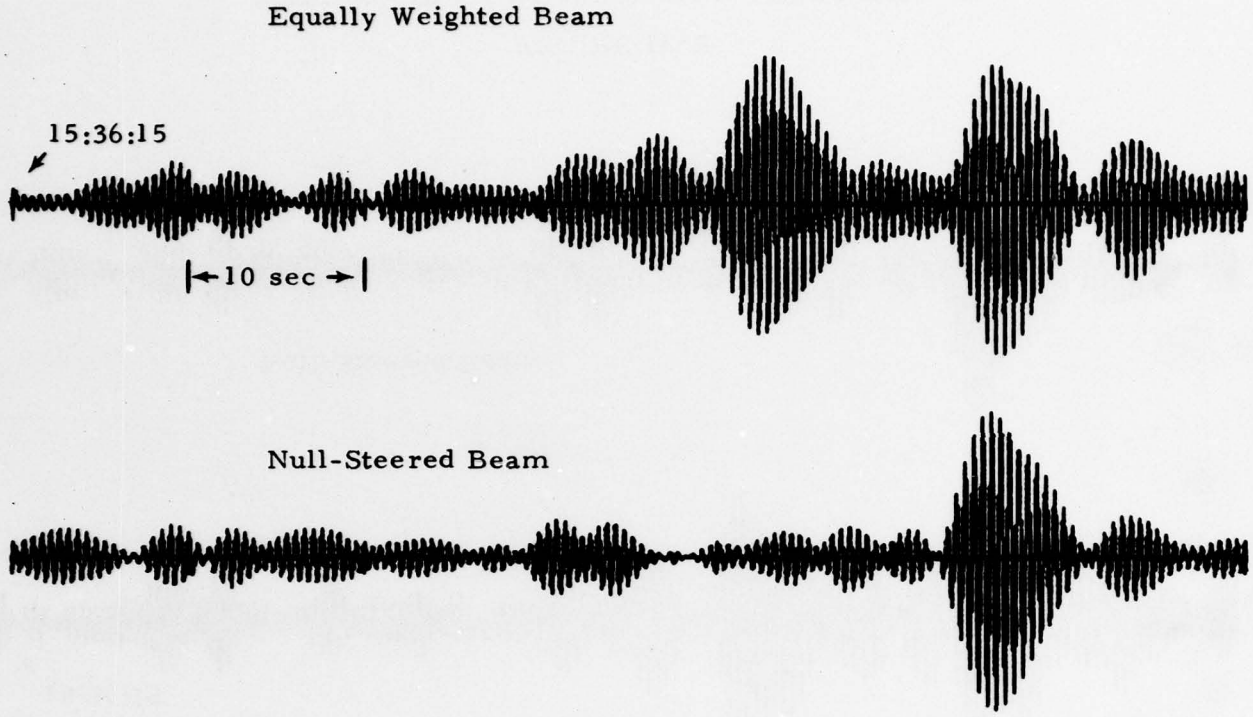

FIGURE IV-7

REAL-AMPLITUDE WEIGHTED ARRAY BEAMS
(f_c = 2.0, Δf = 0.3 Hz, FILTER WEIGHTS AND
RESPONSE PATTERN IN FIGURE III-3)

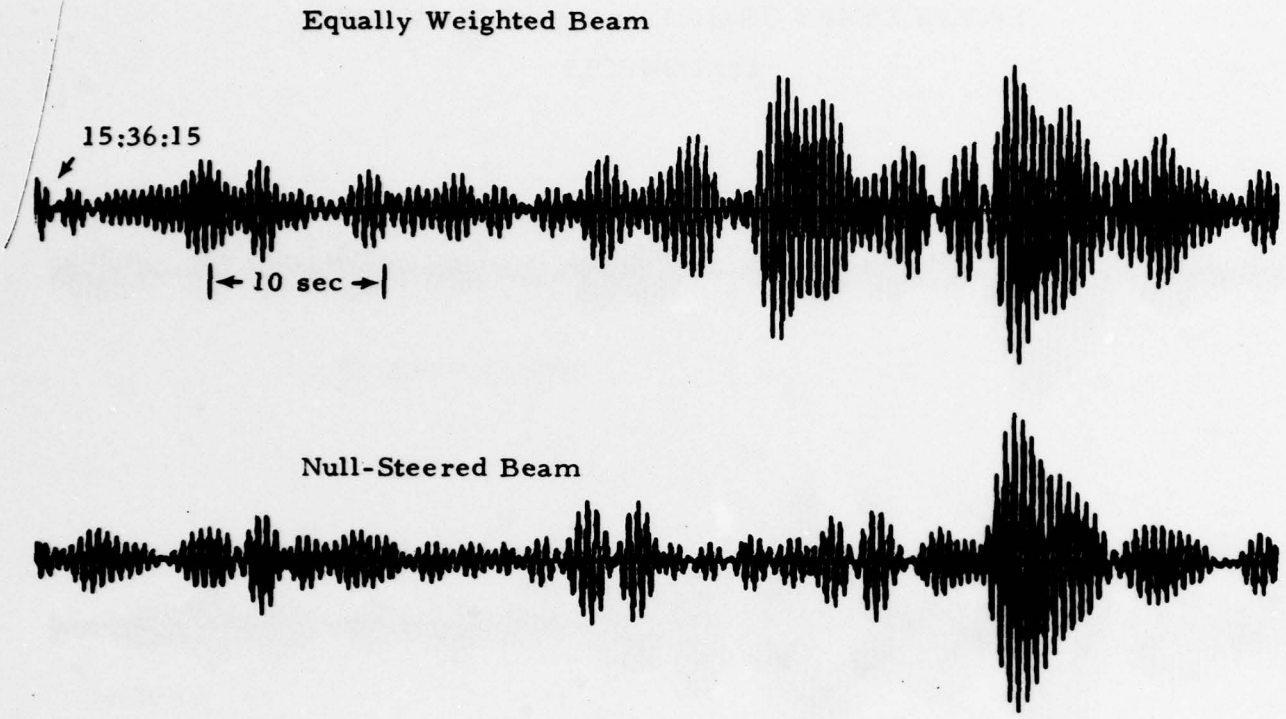

FIGURE IV-8

REAL-AMPLITUDE WEIGHTED ARRAY BEAMS
(f_c = 2.0 Hz, Δf = 0.5 Hz, FILTER WEIGHTS AND
RESPONSE PATTERN IN FIGURE III-3)

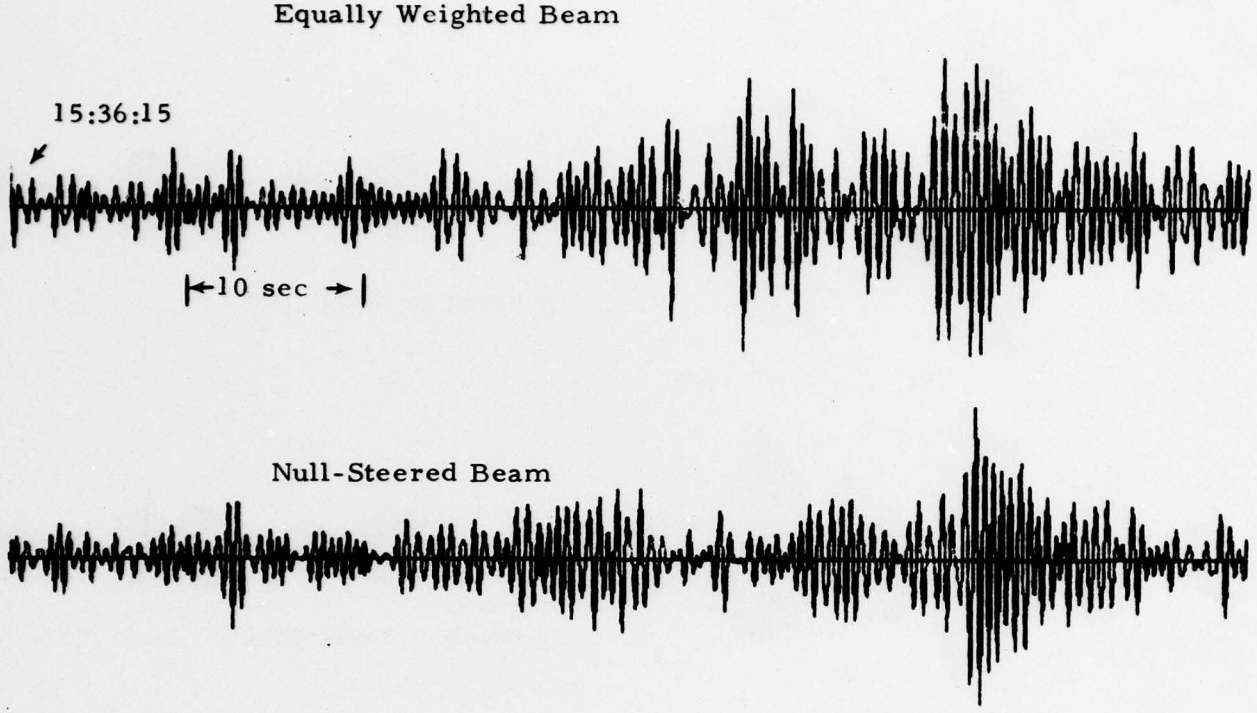

FIGURE IV-9

REAL-AMPLITUDE WEIGHTED ARRAY BEAMS
(f_c= 2.0 Hz, Δf = 1.0 Hz, FILTER WEIGHTS AND RESPONSE PATTERN IN FIGURE III-3)

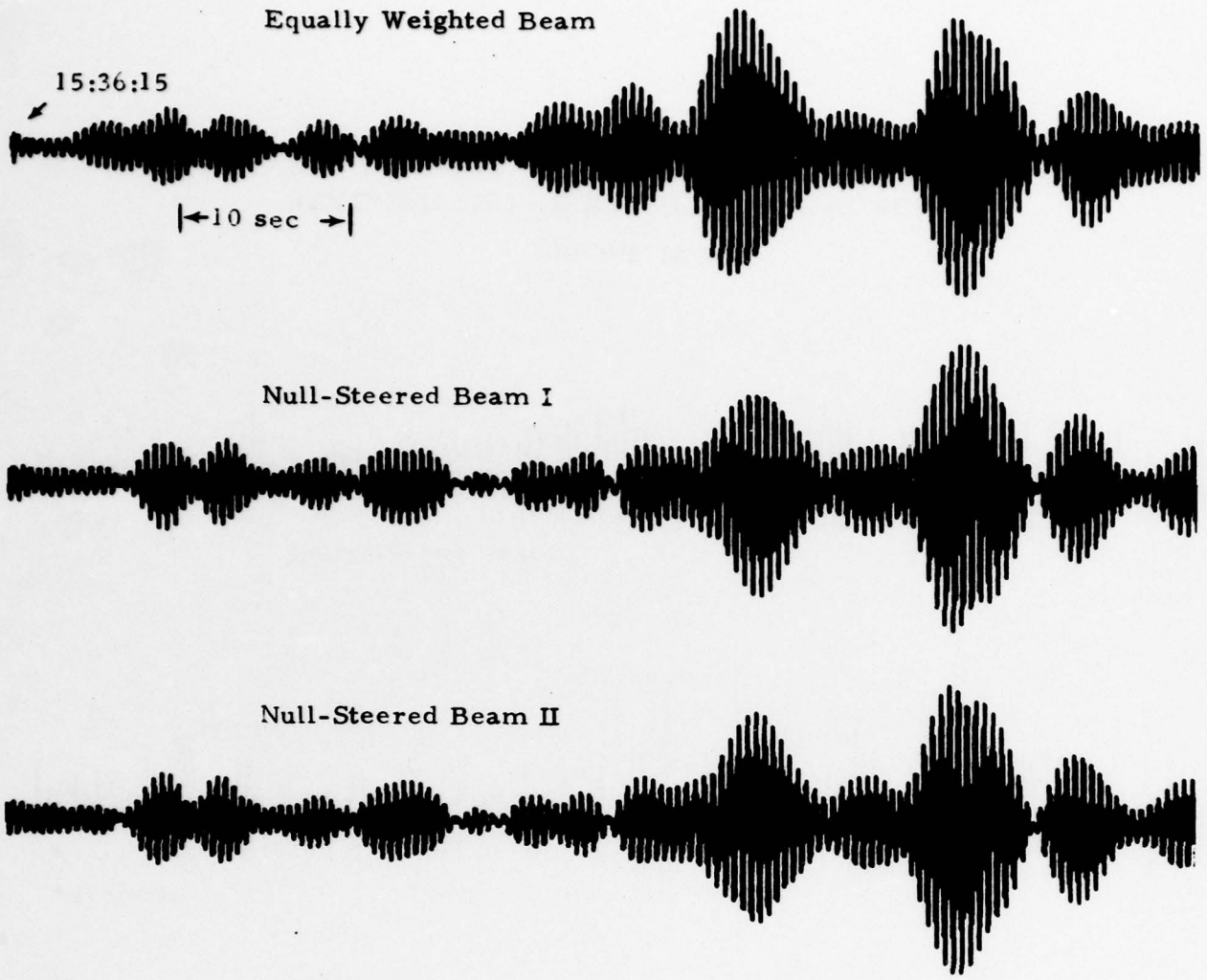

FIGURE IV-10

COMPLEX-WEIGHTED ARRAY BEAMS (f_c = 2.0 Hz, Δf = 0.3 Hz, FILTER WEIGHTS IN TABLE III-3 TRACE 2 BY (a) AND TRACE 3 BY (b))

and the third trace is also the null-steered beam with filter weights in set (b) of the same table. Both filter weight constraint conditions had the same response pattern (Figure III-5) and consistently resulted in the same beam outputs (from a visual point of view). Figure IV-10 had channel data input the same as in Figure IV-7, namely, f_c = 2.0 Hz, Δf = 0.3 Hz. However, the complex weighting algorithm in this case failed to effectively remove the interfering signal from the Ceram Sea while it succeeded in the real-amplitude algorithm shown in Figure IV-7. However, it reduced the interfering signal wavetrains somewhat.

The same complex filter weights in Table III-3 were applied again to the mixed-signal composite array data with slightly increased bandwidth as it was done in the real-amplitude algorithm. Figure IV-11 shows the array beams in which bandpass parameters were: f_c = 2.0 Hz, and Δf = 0.5 Hz. The rejection of interfering energy deteriorated. The experiments were carried out to the bandwidth of 2.0 Hz signal for this case and Figure IV-12 displays its outputs where f_c = 2.0 Hz and Δf = 1.0 Hz. The experimental results totally failed to reduce the null-steered signal in this case.

D. SUMMARY

Using the same composite set of the stronger interfering signal and the weaker desired signal data, the experimental work of mixed signal separation was carried out by applying the ABF processor and optimum array shading techniques to the mixed-signal data.

The adaptive beamforming of time-domain data can be used as a front-end detector or estimator. In a detection system, only azimuth and velocity are needed to steer the array which can be fixed to cover selected areas of interest. Test results from the mixed signal case indicated that the ABF was successful in eliminating the interfering energy and in extracting the desired weak signal to the level that a detection can be claimed.

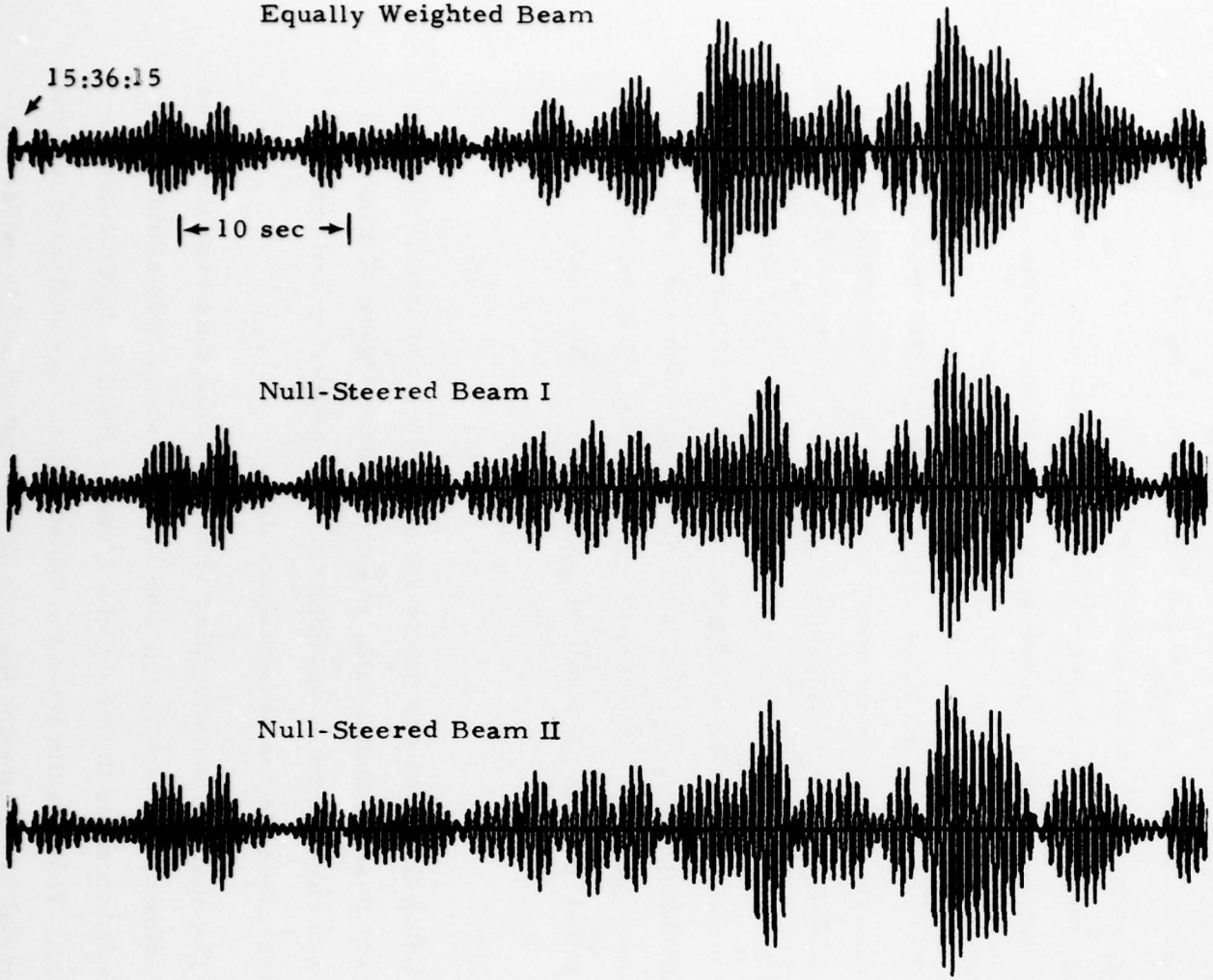

FIGURE IV-11

COMPLEX-WEIGHTED ARRAY BEAMS (f_c = 2.0 Hz, Δf = 0.5 Hz, FILTER WEIGHTS IN TABLE III-3 TRACE 2 BY (a) AND TRACE 3 BY (b))

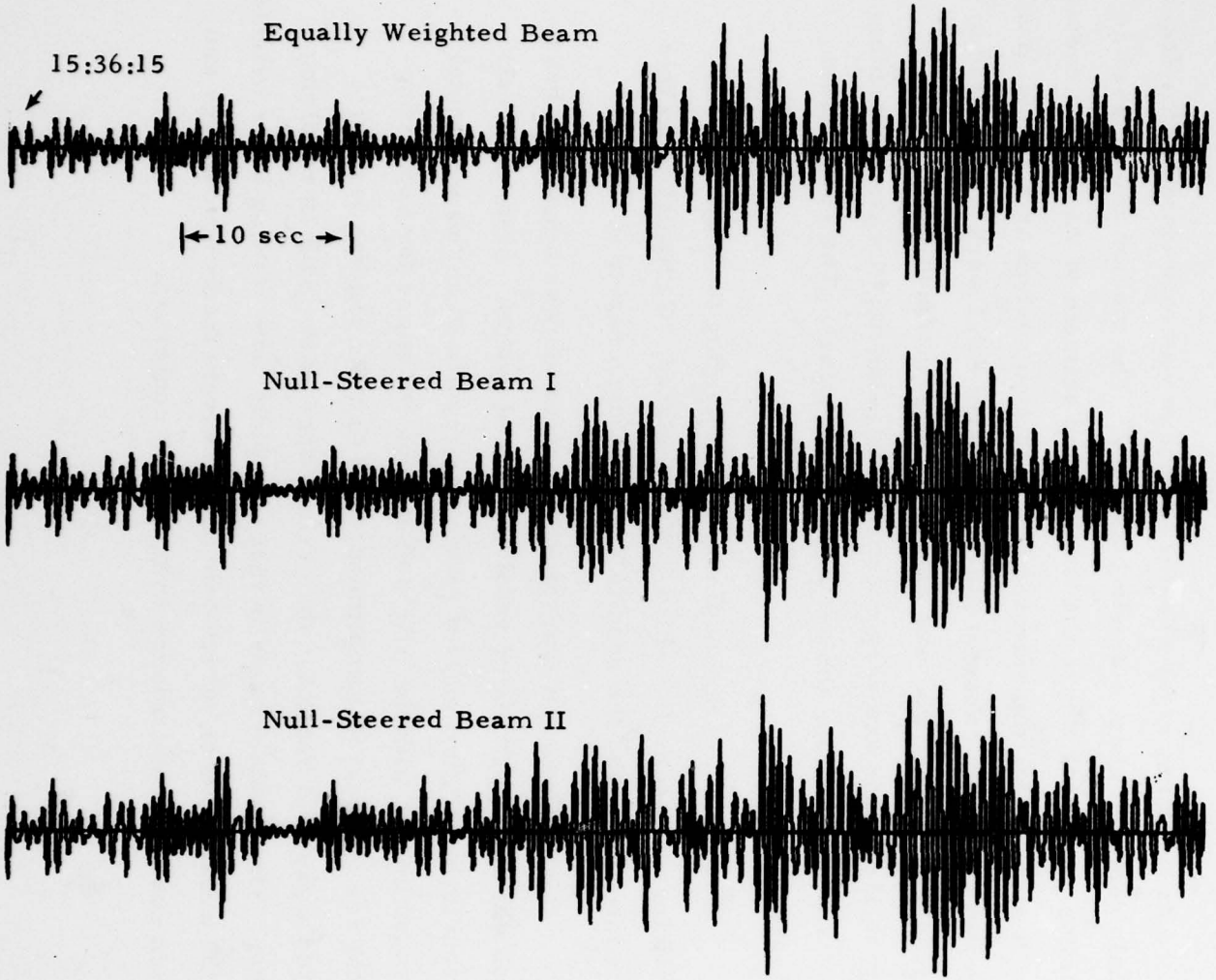

FIGURE IV-12

COMPLEX-WEIGHTED ARRAY BEAMS (f_c = 2.0 Hz, Δf = 1.0 Hz, FILTER WEIGHTS IN TABLE III-3 TRACE 2 BY (a) AND TRACE 3 BY (b))

Experiments in various passbands, narrow and wide, suggested that the ABF processor was a powerful method for a front-end detection system, with considerable capability for resolving mixed events.

An optimum array shading technique was formulated in the frequency domain centered about a single frequency. The method can be used as a post-detection processor where the velocity and azimuth of interfering events are known. It also can be implemented in a detection system as a special processor to reject the highly coherent noise. Experimental work was limited to the single-frequency design that was applied to a narrowband signal. The real-amplitude algorithm was very successful in removing the stronger interfering signal and in enhancing the desired weaker signal. The results seem to be encouraging.

However, the optimum complex weighting technique did not yield the anticipated results for which it was designed. Computation in this algorithm is laborious, and the results were not encouraging at all.

In short, we felt that the ABF processor was a powerful beamforming tool with the capability of resolving mixed events. Also, the real-amplitude shading algorithm yielded promising results in our experimental test. The experiments with the ABF and shading technique for separating mixed events are considered complimentary in that the shading technique demonstrates a physical basis for the performance of the ABF in resolving mixed events. The physical basis is that of rapidly time varying filter weights applied to the array channel, which void out relatively incoherent energy and pass coherent energy in accordance with Levin's constraint.

SECTION V
CONCLUSION AND SUGGESTION

A. CONCLUSION

The physical problem of mixed-signal situations we have tried to solve is to separate, to detect, and to extract the weaker signal hidden in the stronger wavetrains of an earthquake. Being able to detect weaker signals increases the detection capability of an array and being able to extract lower amplitude signal waveforms from much higher amplitude interfering coherent wavetrains also enhances the discrimination capacity of the array.

We have developed two array beamforming methods for the mixed-signal separation problem. One is the time-domain adaptive beamforming filter and the other the frequency-domain array shading (weighting) technique. Both methods apply the variational principle of mathematical physics. However, the ABF is in the time-domain and data-iterative, requires neither a priori noise statistics nor signal information and can be implemented in real-time processing. The array shading technique is in the frequency-domain design, needs information of interfering azimuth, and must be used in a post-detection processor.

Using the recorded data from the KSRS short-period array, a composite data tape was formed to simulate the recorded mixed signal data by adding the data of high amplitude signal wavetrains from a seismic event in the Ceram Sea to those of a low amplitude signal (noise level) from a seismic event in Tadzhik. The ABF processor outputs in wide band (0.5-3.5 Hz) and in narrow bands (0.5-1.5 Hz, and 1.5-2.5 Hz) showed that the interfering wavetrains were successfully eliminated and the desired weak signal

was clearly enhanced to a detectable level, while the desired signal in beam-steer outputs was at the level of interfering wavetrains and was non-detectable. The experimental test of the real-amplitude shading algorithm indicated that the results were promising and deserves further study. However, the complex-shading algorithm did not yield the satisfactory results predicted from beam pattern computation. Real amplitude weighting appears to be a sufficient tool for studying mixed-signal problems.

In conclusion, we felt that the present ABF is a powerful real-time array processor and the real-amplitude shading technique could be useful for post-processing the coda of large signals.

B. SUGGESTION FOR FURTHER STUDY

The ABF could be improved to speed-up the computation. Technical aspects for practical implementation as a real-time detector are currently being studied. A detailed presentation of detection performance will be in a separate report (Shen, 1978) where it was tested on a large ensemble of events.

The preliminary experimental results suggest that real-amplitude shading techniques are potentially useful for removing the coherent interfering energy and for extracting a hidden signal in a coherent interfering environment. A useful approach would be to bury a signal from an underground nuclear explosion in various types of interfering environments. A systematic study could be made and a set of filter weights could be designed from the study so that they could be used for post-detection searches for hidden explosions or other research purposes.

The real-amplitude shading algorithm was formulated for a single-frequency signal that was applied to a relatively narrowband signal. A wide band signal can be synthesized by summing the data of various

narrowband signals in the frequency domain. To evaluate its practical usefulness, research of this sort should be conducted.

Extension of the present work to long-period seismic array data for surface wave extraction would be useful for both detection and discrimination research.

SECTION VI
REFERENCES

Burg, J. P., A. H. Booker, and M. Holyer, 1967; Adaptive Filtering of Seismic Array Data, Advanced Array Research, Report No. 1, Texas Instruments Incorporated, Science Services Division, Dallas, Texas and a number of technical reports by Booker and his co-workers.

Dolph, C. L., 1946; A Current Distribution for Broadside Arrays, Inst. Radio Engrs., 34, 335-348.

Frost, O. L. III, 1972; An Algorithm for Linearly Constrained Adaptive Array Processing, Proceedings of the IEEE, vol. 60, No. 8, 926-935.

Gangi, A. F., and B. S. Byun, 1976; The Corrective Gradient Projection Method and Related Algorithms Applied to Seismic Array Processing, Geophysics, vol. 41, No. 5, 970-984.

Kobayashi, H., 1970; Iterative Synthesis Methods for a Seismic Array Processor, IEEE Transactions on Geoscience Electronics, vol. GE-8, No. 3, 169-178.

Levin, M. J., 1964; Maximum-Likelihood Array Processing, in M. I. T. Lincoln Laboratory Semi-Annual Technical Summary Report, DDC455743.

Owsley, N., 1973; A Recent Trend in Adaptive Spatial Processing for Sensor Arrays: Constrained Adaptation, in Signal Processing, edited by J. W. R. Griffiths, P. L. Stocklin, and C. van Schooneveld, Academic Press, New York, NY.

Shen, W. W., 1977; Study of Adaptive Beamforming Algorithms for Low Magnitude Seismic P-wave Detection, Technical Report No. 5, Texas Instruments Report No. ALEX(01)-TR-77-05, AFTAC Contract Number F08606-77-C-0004, Texas Instruments Incorporated, Dallas, TX.

Shen, W. W., 1978; Detection Performance of Time-Varying Adaptation Rate Adaptive Beamformer, in preparation.

Wang, H. S. C., 1975; Amplitude Shading of Sonar Transducer Arrays, J. Acoust. Soc. Am., 57, 1076-1084.

Wang, H. S. C., 1977; Interference Rejection by Amplitude Shading of Sonar Transducer Arrays, J. Acoust. Soc. Am., 61, 1251-1259.